


Summer Greenland Blocking in reanalysis and in SEAS5.1 seasonal forecasts: robust trend or natural variability?

Johanna Beckmann^{1,2,R}, Giorgia Di Capua^{2,R}, Paolo Davini³

¹School of Earth, Atmosphere and Environment, and ARC Special Research Initiative for Securing Antarctica’s Environmental Future, Monash University, Clayton, Kulin Nations, Australia.
²Earth System Analysis, Potsdam Institute for Climate Impact Research, Member of the Leibniz Association, Potsdam, Germany
³Consiglio Nazionale delle Ricerche, Istituto di Scienze dell’Atmosfera e del Clima, Torino, Italy

 shared first authorship

Correspondence to: Giorgia Di Capua (dicapua@pik-potsdam.de)

Abstract. Given its impact on enhanced melting of the Greenland ice sheet, it is crucial to assess changes in frequency and characteristics of summer Greenland blocking. Indeed, the occurrence of such atmospheric patterns has seen a marked increase in recent decades. However, the observed trend is not captured by any simulation from state-of-the-art global climate models. It is therefore paramount to determine whether the lack of trend is caused by a misrepresentation of key physical mechanisms in climate models or whether such trend is mainly attributable to decadal variability, or both. Here we investigate Greenland blocking characteristics in reanalysis (ERA5) and ECMWF seasonal forecasts (SEAS5.1), showing that about 10% of the 1000 permutations of SEAS5.1 runs can simulate a 43-year trend equal or larger to the ERA5 one: this suggests that the initialization and the higher model resolution contribute to a more realistic representation of the blocking dynamics than in freely-evolving climate model runs. To further investigate these aspects, we apply the Peter and Clark momentary conditional independence (PCMCI) algorithm to assess monthly causal pathways. Results show that while the relationship among Arctic temperature, snow cover, Atlantic multidecadal variability and Greenland blocking is consistent both in ERA5 and SEAS5.1, the effect of early snow melt over North America on Greenland blocking is mostly absent in SEAS5.1. Therefore, while it is possible that the observed trend is due to internal decadal variability, the misrepresentation of the snow cover processes may explain the difficulty that SEAS5.1 has in reproducing the observed trend. This deficit in representing the snow impact on the atmospheric circulation might also be the culprit of the missing trend in climate models, raising the question whether long-term projections underestimate a future increase in Greenland blocking and ice sheet melt.

Style Definition: Normal

Style Definition: Heading 1

Style Definition: Heading 2

Style Definition: Heading 3

Style Definition: Heading 4

Style Definition: Bullets: Outline numbered + Level: 1 + Numbering Style: 1, 2, 3, ... + Start at: 1 + Alignment: Left + Aligned at: 0 cm + Tab after: 1.27 cm + Indent at: 1.27 cm

Deleted: observations

Formatted: Font: 17 pt, Bold, Font colour: Black

Formatted: Font: 17 pt, Bold, Font colour: Black

Formatted: Normal, Space Before: 18 pt, Line spacing: Multiple 1.83 li, Border: Top: (No border), Bottom: (No border), Left: (No border), Right: (No border), Between : (No border)

Deleted: Beckmann¹

Deleted: ¹,

Deleted: Capua²⁺,

Formatted: Font: 12 pt, Font colour: Black, English (UK)

Formatted: Font: Cardo, 12 pt, Font colour: Black, English (UK)

Formatted: Font: 12 pt, Font colour: Black, English (UK)

Formatted: Font: 12 pt, Font colour: Black, English (UK)

Formatted: Font colour: Black

Formatted: English (UK)

Deleted: ⁺

Formatted: Font colour: Black

Formatted: Normal, Space Before: 6 pt, After: 18 pt, Border: Top: (No border), Bottom: (No border), Left: (No border), Right: (No border), Between : (No border)

Deleted: pattern

Deleted: : however

Deleted: 1[†]

Formatted: Font colour: Black

Formatted: Normal, Border: Top: (No border), Bottom: (No border), Left: (No border), Right: (No border), Between : (No border), Tab stops: 7.96 cm, Centred + 15.92 cm, Right

37 **1 Introduction**

38 ~~Atmospheric blocking over Greenland can be defined by the occurrence of a persistent anticyclone in the mid-troposphere in~~
39 ~~proximity to Greenland (Hanna et al. 2016). More precisely, it is a large-scale atmospheric high-pressure low-vorticity system~~
40 associated with the negative phase of the North Atlantic Oscillation (Woollings and Hoskins, 2008).

41 Despite being less studied than its winter counterpart, summer Greenland blocking presents characteristics that can severely
42 impact the Greenland ice sheet ~~which has recently put it at the center of the scientific community attention~~ (Hanna et al., 2018;
43 McLeod and Mote, 2016; Tedesco and Fettweis, 2020, ~~Wang and Luo, 2022~~). Due to its anticyclonic structure, during periods
44 of strong Greenland blocking southerly advection of warm air on the western side of Greenland favours enhanced melting
45 (McLeod and Mote, 2016). Indeed, blocking has been associated with extreme melt years ~~of recent years~~ (Tedesco et al., 2011,
46 Nghiem et al., 2012, Tedesco and Fettweis, 2020). Moreover, modelling studies ~~suggest~~ that if these extreme melting years
47 increase in frequency in the future, the contribution to sea level rise from the Greenland Ice Sheet could increase by 20% by
48 the end of the 23rd century (Beckmann and Winkelmann, 2023).

49 ~~Most importantly, multiple evidence is accumulating in recent years showing that the frequency of occurrence of summer~~
50 ~~Greenland blocking has been increasing in the last two decades (Hanna et al., 2018; Wachowicz et al., 2021). This is most~~
51 ~~relevant considering the fact that state-of-the-art climate models seem to lack agreement with the observed positive blocking~~
52 ~~trends for summer Greenland blocking, questioning whether projected future changes for blocking – and indirectly for ice~~
53 ~~sheet melting - are reliable (Davini and D’Andrea, 2020; Delhasse et al., 2020; Maddison et al., 2024; Masato et al., 2013).~~
54 ~~Despite being weaker in summer months,~~ Arctic amplification (AA), i.e. the phenomenon that sees the Arctic region warming
55 at a pace two-to-four times faster than the rest of the Northern Hemisphere (Cohen et al., 2014; Davy et al., 2018; Previdi et
56 al., 2021; Serreze et al., 2009) has been suggested to influence circulation patterns in the northern mid-latitudes ~~and possibly~~
57 ~~influence blocking~~ (Cohen et al., 2014; Francis and Skific, 2015; Nakamura et al., 2016): enhanced Arctic warming can affect
58 weather patterns, leading to weaker storm tracks, shifts in the position of the jet stream and favouring the amplification and
59 persistence of Rossby waves (Coumou et al., 2018).

60 However, a clear understanding of the underlying mechanisms leading to ~~the observed Greenland blocking~~ increase is not yet
61 available. Preece et al. (2023) proposed a mechanism which connects reduced snow cover in late spring over the North
62 American continent with the formation of a Rossby wave pattern, which in turn enhances blocking over Greenland in the
63 following summer. However, the large interannual variability of the region, which is often described as a red noise process
64 (Feldstein, 2000) and can present years of extremely high blocking frequency followed by years where almost no blocking is
65 observed, still questions the real presence of a long-term trend (Davini et al., 2021; Gollan et al., 2015). For example, in recent
66 years the trend of Greenland blocking has weakened (Preece et al., 2023) leaving open the ~~possibility that the increase is a~~
67 ~~consequence~~ of natural variability. ~~In this direction, natural~~ climate variability modes, such as the Atlantic Multidecadal
68 Variability (AMV), may impact large scale circulation patterns in the North Atlantic, and the local jet stream dynamics, thus

Deleted: Atmospheric blocking over Greenland can be defined by the presence of a persistent anticyclone in the mid-troposphere in proximity of Greenland. In the boreal summer, it is accompanied by higher than average temperature anomalies at the surface which can significantly contribute to melting of the Greenland ice sheet (Hanna et al., 2014; Tedesco and Fettweis, 2020; Wang and Luo, 2022). The years 2012 and 2019, which rank first and second respectively for negative surface mass balance over the Greenland ice sheet (Tedesco and Fettweis, 2020) encapsulate the essence of such a process. In both years, persistent blocking patterns triggered extreme melting, reaching even the ice sheet’s summit. While anthropogenic global warming increases the mean temperature of the troposphere, changes in the frequency and intensity of key atmospheric patterns, such as the Greenland blocking pattern can further enhance melting at the surface (McLeod and Mote, 2016

Moved down [1]: ; Wachowicz et al., 2021).

Moved down [2]: 2020; Maddison et al., 2024; Masato et al., 2013).

Deleted: Thus, such changes pose an additional threat to the stability of the ice sheet itself and may lead to additional sea level rise (Beckmann and Winkelmann, 2023; Sasgen et al., 2020; Shepherd, Andrew et al., 2021). It is then crucial to establish whether climate models can correctly represent the physical mechanisms that lead to blocking in historical simulations, to gain confidence that future projections do not underestimate the effect of atmosphere ... [2]

Deleted: Greenland blocking

Deleted:) located over Greenland. Given its large spatial scale of thousands of km, Greenland blocking can have a large impact ... [3]

Deleted:), a phenomenon that has gained relevance in recent years.

Deleted: in 2010

Deleted:), 2012 (

Deleted:), and 2019 (

Deleted:) and can generally lead to significant summer temperature anomalies (Blau et al., 2024).

Deleted: show

Moved (insertion) [1]

Moved (insertion) [2]

Deleted:), however with contrasting results (Blackport and Screen, 2020; Cohen et al., 2020; Screen et al., 2018). While the AA s ... [4]

Deleted: in summer

Deleted: Changes in atmospheric circulation patterns in the North Atlantic sector connected to AA can affect the frequency and ... [5]

Deleted: such

Deleted: opportunity of being a result of

Deleted: signal

Deleted: Natural

Deleted: 2

Formatted: Font colour: Black

Formatted

... [1]

indirectly affecting blocking onset and maintenance, and further complicating the scenario (Häkkinen et al., 2011; Luu et al., 2024).

Beyond high- and mid-latitude drivers, tropical sea surface temperatures and convection can affect summer climate over Greenland and the Arctic, including Rossby wave trains that enhance sea ice melt (Baxter et al., 2019). Model experiments forced with tropical sea surface temperatures show that anomalies in mid-to-upper-tropospheric anticyclonic wind may explain half of the observed Greenland surface warming and ice loss acceleration over the last three decades (Topál et al., 2022).

Another element which further tangles up the Greenland blocking puzzle is related to its representation in climate models. Despite modeling blocking has always been a challenge for both numerical weather prediction models and global climate models, significant improvements have been achieved in the last 25 years (Davini and D'Andrea, 2016, 2020). However, evidence is emerging that none of the Coupled Model Intercomparison Project - Phase 5 (CMIP5) and Phase 6 (CMIP6) models, among the hundreds of ensemble members available, is capable of replicating the observed increasing trend of summer Greenland blocking, and neither project a significant increase until 2100 (Delhasse et al., 2020; Luu et al., 2024; Maddison et al., 2024). Moreover, CMIP6 models also fail to capture the magnitude of the melting events, such as the one observed in summer 2019, hinting at a potential underestimation of ice sheet mass loss over Greenland (Delhasse et al., 2020).

Such lack of trends questions the capability of CMIP6 models to capture features such as the Arctic amplification and significantly weakens the reliability of their climate predictions. In this context, identifying the atmospheric and surface drivers of Greenland blocking variability, both in observations and general circulation models, can help assess which physical mechanisms govern the variability of Greenland blocking and which of the identified mechanisms can be confidently reproduced by climate models.

Causal discovery can help identify causal relationships in a set of different climate and atmospheric variables (Di Capua et al., 2020b; McGraw and Barnes, 2020; Runge et al., 2019a), and provides a tool to validate model performance in reproducing atmospheric causal pathways (Di Capua et al., 2023; Nowack et al., 2020). The Peter and Clark momentary conditional independence (PCMCI) algorithm is a causal discovery tool that helps identify true causal relationships from spurious correlation values (Runge, 2018; Runge et al., 2019a, b). With respect to other causal discovery tools, such as Granger causality, PCMCI allows us to assess the possible effect of a (set of) third variable(s). However, when compared to other causal discovery techniques, such as the Liang–Kleeman information flow, PCMCI yields very compatible results, thus providing a robust tool for the identification of causal relationships (Docquier et al., 2024). PCMCI has found several applications in the field of climate and atmospheric sciences, ranging from the identification of tropical – extratropical teleconnections in observations and forecasting models (Di Capua et al., 2020a, 2023) to stratospheric pathways leading to sudden stratospheric warming events (Kretschmer et al., 2016, 2018a), climatological variability (Di Capua et al., 2019; Lehmann et al., 2020; Pfleiderer et al., 2020), and much more (Tian et al., 2024; Di Capua et al., 2024).

In the current work, we aim at investigating the Greenland blocking representation in state-of-the-art multi-member high-resolution monthly-initialized seasonal forecast system, namely the European Centre for Medium-range Weather Forecasts (ECMWF) SEAS5.1 forecast system, to understand to what extent, initialization characteristics and high resolution could help

Deleted: Next to high- and mid-latitude drivers, tropical sea surface temperatures and convective activity in the tropical belt can provide further physical mechanisms that can potentially affect warming trends and blocking features over Greenland and the Arctic region (Gan et al., 2024; Liu et al., 2016; Matsumura and Kosaka, 2019). In winter, El Niño episodes and anomalous sea surface temperatures in the tropical Pacific can affect surface warming in the Arctic region via a Rossby wave response (Ding et al., 2014; Matsumura and Kosaka, 2019). In summer, a similar mechanism can lead to the formation of Rossby wave trains originating in east-central tropical Pacific, that propagate to the Arctic region enhancing sea ice melting in the Arctic Ocean in September (Baxter et al., 2019). However, central Pacific El Niño events may be responsible for intensified cyclonic circulation over Greenland in summer and lead to surface cooling (Matsumura et al., 2021). Similarly, Hu et. Al (2016) show that central Pacific El Niño events can strengthen the tropospheric Arctic polar vortex and the circumpolar westerly wind, which can contribute to inhibiting Arctic warming and sea-ice melting in summer....

Deleted: , leading to better representation of the patterns, frequency and trends of blocking

Deleted: Higher resolution and improved physical mechanisms have lowered the chronic circulation biases that general circulation models reported on the Euro-Atlantic sector and have thus improved their ability of representing blocking – from a climate point of view – in a fairly good way.

Deleted: 2024). Such lack of trends questions the capability of CMIP6 models to capture the signal of the Arctic amplification and significantly weakens the reliability of their climate predictions. ¶

Deleted: 2020). However, if climate models fail to reproduce observed changes (Hanna et al., 2018), then the question whether projected future changes are realistic and reliable remains open.

Deleted: Moreover, it is yet unclear whether the observed trend in Greenland blocking is robust across different observational datasets and over different time periods.

Deleted: identifying

Deleted: casual

Deleted: identifying

Deleted:),

Deleted: and forecasting of crop yields, hurricanes and Indian summer monsoon rainfall

Deleted: historical drivers of compound hot and dry extreme events in central Europe

Deleted: accepted) to the identification of local and remote atmospheric drivers of circulation variability in the eastern Mediterranean (...)

Deleted: 3¶

Formatted: Font colour: Black

Formatted: Normal, Border: Top: (No border), Bottom: (No border), Left: (No border), Right: (No border), Between : (No border), Tab stops: 7.96 cm, Centred + 15.92 cm, Right

227 in capturing the observed summer Greenland blocking trend. Robustness of the **blocking** climatology of SEAS5.1 has been
228 already assessed (Davini et al., 2021), so that this will help us disentangling the role of natural variability from that of
229 anthropogenic climate change in affecting the variability and trends of Greenland blocking, hence helping to resolve a piece
230 of the complex puzzle of Greenland blocking trend. The remainder of this manuscript is organized as **follows**: we first describe
231 the data and method used (Sect. 2), then present the results obtained (Sect. 3) and finally discuss the results (Sect. 4).

232 **2 Data and Methods**

233 **2.1 Data**

234 We **analyse** daily atmospheric fields and snow cover fields during the boreal summer period (June to August, JJA) using
235 gridded data (0.25°x0.25° spatially **regridded** to 1°x1°) for the period 1940-2023 from the ERA5 reanalysis dataset (Hersbach
236 et al., 2020) and for the period 1981-2023 from the SEAS5.1 seasonal **forecast** dataset (Johnson et al., 2019), both provided
237 by the European Centre for Medium-range Weather Forecasts (ECMWF). Specifically, we consider daily (temporally averaged
238 to obtain monthly samples) geopotential height at 500 hPa (Z500), 2m temperature (T2m), snow cover (Snow), sea surface
239 temperature (SST) and mean sea level pressure (MSLP). Snow is obtained from snow density and snow depth fields (see Text
240 S1 in the Supplementary Material). **For** ERA5, we use the entire 1940-2023 period (referred in the text as ERA5-40) to assess
241 long term trends. However, for the most part of the analysis we use the 1981-2023 period (ERA5-81), to allow a direct
242 comparison with the SEAS5.1 dataset. **To focus on dynamic linkages**, for each of the **three** monthly time steps considered in
243 each JJA season, the trend over the 43 years for ERA5-81 (or 84 years for ERA5-40) is removed and anomalies around zero
244 are calculated, thus removing both the trend and seasonal cycle. Note that data are not detrended when historical trends are
245 analysed.

246 SEAS5.1 initialized on March 1 (SEAS5.1-03), May 1 (SEAS5.1-05) and June 1 (SEAS5.1-06) have been used. Although
247 SEAS5.1 provides 51 ensemble members, 25 ensemble members each year are publicly available through the Copernicus
248 Climate Data Store, thus a total of 25x43 (1075) model years. SEAS5.1 data are extracted from the initialization date **until**
249 October 1, thus a total of seven, five and four months are available for SEAS5.1-03, SEAS5.1-05 and SEAS5.1-06 respectively.
250 As for ERA5, also for SEAS5.1 data, we provide monthly averages, remove the trend over the 1981-2023 period and calculate
251 anomalies centred around zero.

252 **2.2 Greenland blocking indices**

253 Atmospheric blocking can be detected in several ways which can lead to apparently contradictory results, strongly affected by
254 the index chosen for **its** identification (Woollings et al., 2018). As for other blocking regions, multiple approaches have been
255 proposed to identify the blocking anomaly over Greenland (Hanna et al., 2016, 2018; Wachowicz et al., 2020). In the current
256 work, we adopt an atmospheric blocking index which follows the original definition by Tibaldi and Molteni (1990) but
257 extended to a 2-D field following Scherrer et al. (2006) and Davini et al (2012a). This is an index based on the reversal of the

Deleted: follow

Deleted: analyse

Deleted: averaged

Deleted: retrospective

Deleted: To focus on dynamic linkages, the interannual variability, seasonal cycle and any long-term trend are removed (unless otherwise specified).

Deleted: For

Deleted: 3

Deleted: (84)

Deleted: till

Deleted: Linear correlation analysis and probability-trend estimation were conducted for all datasets mentioned. The correlation and causal inference analyses were performed for both SEAS5.1-03 and SEAS5.1-05, except for the causal effect networks (CEN). For causal discovery, only SEAS5.1-03 was used, as the absence of March and April data in SEAS5.1-03 violates PCMCI algorithm requirements (see Section 2.3 for details).

Deleted: ¶

Deleted: their

Deleted: .,

Deleted:).

Deleted: 4¶

Formatted: Font colour: Black

Formatted: Normal, Border: Top: (No border), Bottom: (No border), Left: (No border), Right: (No border), Between : (No border), Tab stops: 7.96 cm, Centred + 15.92 cm, Right

meridional gradient of the Z500 field: in contrast to other indices based on anomaly measures, it targets the presence of easterly winds to the south of the blocked grid point, providing a dynamical relevant definition of the phenomenon. To define the index, two meridional geopotential height gradients at southern (GHGS) and northern (GHGN) latitudes are defined:

$$GHGS(\lambda_0, \varphi_0) = \frac{Z500(\lambda_0, \varphi_0) - Z500(\lambda_0, \varphi_S)}{\varphi_0 - \varphi_S}, \tag{1}$$

$$GHGN(\lambda_0, \varphi_0) = \frac{Z500(\lambda_0, \varphi_N) - Z500(\lambda_0, \varphi_0)}{\varphi_N - \varphi_0}, \tag{2}$$

where φ_0 ranges from 30° to 75°N and λ_0 ranges from 0° to 360°E. $\varphi_N = \varphi_0 + 15$ and $\varphi_S = \varphi_0 - 15$, such that the gradients are always calculated 15° North and 15° South of φ_0 . The GHGS index defines where the reversal is happening, and it is the key element for the identification of blocking. GHGN ensures the presence of westerly winds northward to the blocked area, focusing on the presence of a high-pressure dome over the analysed region. To ensure that the blocking index is not detecting a poleward migrating subtropical ridge – a condition typically occurring in summer months in Northern Hemisphere (i.e. that easterly winds are not caused by trade winds), a supplementary definition from Davini et al. (2012a) is introduced, and named $GHGS_2$:

$$GHGS_2(\lambda_0, \varphi_0) = \frac{Z500(\lambda_0, \varphi_S) - Z500(\lambda_0, \varphi_{S_2})}{\varphi_S - \varphi_{S_2}}, \tag{3}$$

Where $\varphi_{S_2} = \varphi_S - 15^\circ$.

Consequently, at daily time scales, blocking is thus identified when:

$$GHGS(\lambda_0, \varphi_0) > 0,$$

$$GHGN(\lambda_0, \varphi_0) < -\frac{10m}{^\circ lat}$$

$$\text{and } GHGS_2(\lambda_0, \varphi_0) = -\frac{5m}{^\circ lat}$$

Blocking is thus a binary index, which can be spatially averaged over Greenland (55°W-0°, 67°N-75°N) to produce what we define as the Greenland blocking index (GBI). Note that the GBI region is identified based on where a significant positive trend in the 2-D blocking index is detected (Fig. 1a).

However, such a binary index focuses on the exceptional non-linearity of blocking itself. Given that the target of this analysis is the long-term trend in the strength and shape of geopotential height over Greenland, we also introduce a continuous (non-binary) index, which is obtained as the linear combination of GHGS and GHGN. Indeed, at high latitudes, $GHGS_2$ is found to have a negligible role (not shown). Thus, we define the Greenland gradient index (GGI) so that $GGI = GHGS - GHGN$, which is then highly correlated with GBI. GGI represents an alternative measure to standard blocking and can be physically interpreted as a measure of the strength of the geopotential height anomaly. In both cases – given the limited impact that such

Deleted: condition

Deleted: °.

Deleted: 5

Formatted: Font colour: Black

Formatted: Normal, Border: Top: (No border), Bottom: (No border), Left: (No border), Right: (No border), Between : (No border), Tab stops: 7.96 cm, Centred + 15.92 cm, Right

309 constraint has on the real pattern and frequency of blocking – we followed the approach of previous literature (Davini and
310 D’Andrea, 2020; Tibaldi and Molteni, 1990) and we do not apply any spatial or temporal constraint to the blocking index.
311 Given the wide diversity of possible blocking indices, other alternatives have been explored. The Greenland Blocking Index
312 developed by Hanna et al. (2016), hereafter the HA16 Index, has been computed to provide a sensitivity to an absolute detection
313 method (i.e. not based on gradient reversal). The HA16 Index is a punctual index defined only for Greenland, and it uses the
314 area weighted geopotential height absolute values at 500hPa in the box delimited by 60N-90N, 80W-20W.
315 Similarly, the updated gradient reversal method for high latitude blocking developed by the Tyrliis et al (2021), hereafter the
316 TY21 index, has been computed. This index, which shares with the Davini et al. (2012) method the most of its definitions,
317 loosens the criteria for GHGN asking only to be smaller than 0 for latitude north of 60N. This - according to the authors -
318 allows for a more precise detection of blocking at higher latitude more aligned with blocking detected on isentropic surfaces.

319 **2.3 Causal discovery and causal inference**

320 In the present work, we apply the Peter and Clark momentary conditional independence (PCMCI) algorithm, a causal discovery
321 tool which allows to disentangle spurious from actual *causal* relationships in a set of uni-variate time series. In general, (cross-
322) correlation measures are often used to determine the existence of concurrent behaviour between pairs of time series. However,
323 correlation does not imply causation, and spurious correlations can arise from common effects like (i) the presence of strong
324 auto-correlation in one (or both) time series, (ii) common drivers or (iii) indirect links. Thus, two time series may be both
325 driven by a third time series (common driver) and therefore show a significant correlation even though no real causal link is
326 present. PCMCI deals with these issues by iteratively testing for the presence of significant partial correlations (in the linear
327 framework) between pairs of time series by conditioning on a set of one (or more) further time series.
328 The PCMCI algorithm is composed of two steps, the PC-step and the MCI-step. In the PC-step, the algorithm first identifies
329 all significant lagged (up to a certain prescribed lag t_{\max}) correlations among all possible combinations of time series in the set
330 of time series (actors), e.g. $P = \{A, B, C, D, F\}$. The first set of “potential parents” for each time series is identified, e.g. with
331 $t_{\max} = -3$, $P_A^0 = \{A_{t=-1}, B_{t=-2}, C_{t=-1}, D_{t=-3}, E_{t=-2}\}$. Then, the algorithm tests whether the partial correlation between $A_{t=0}$ and
332 each element x_i in P_A^0 is still significant when conditioning on a combination of the remaining elements $x_j \neq x_i$ in P_A^0 . The
333 partial correlation is calculated by (linearly) regressing $A_{t=0}$ and x_i on x_j , and then taking the correlation of the residuals of
334 $A_{t=0}$ and x_i . If this partial correlation is still significant, then $A_{t=0}$ and x_i , will be considered “conditionally dependent”,
335 meaning that their correlation cannot be explained by the linear combination of x_j . In the PC-step, the number of conditions x_j
336 gradually increases until the number of elements in the set of potential parents P_A^n is equal or smaller than the number of
337 iterations. At the end of the PC-step, each time series in P will have its own set of potential patents, e.g. $P_A^n =$
338 $\{A_{t=-1}, C_{t=-1}, D_{t=-2}\}$ and $P_B^m = \{B_{t=-2}, D_{t=-1}, A_{t=-2}, E_{t=-3}\}$.
339 In the MCI-step, the partial correlation is calculated again between all potential pairs of actors in P . However, this time the
340 partial correlation is only calculated once by conditioning on the common set of parents identified in the PC-step. E.g. if $A_{t=0}$

Deleted: casual

Deleted: 6

Formatted: Font colour: Black

Formatted: Normal, Border: Top: (No border), Bottom: (No border), Left: (No border), Right: (No border), Between : (No border), Tab stops: 7.96 cm, Centred + 15.92 cm, Right

342 and $B_{t=-1}$ are tested, then the partial correlation will be calculated using the joint set of parents of $A_{t=0}$ and $B_{t=-1}$, the latter
343 being equal to the set of parents of $B_{t=0}$ which has been adjusted for lag -1. The actors found to be conditionally dependent in
344 the MCI-step define the set of causal parents for each time series. Finally, the significance of the detected causal links (each
345 partial correlation has its own p -value) is corrected by applying the Benjamini-Hochberg false discovery rate (FDR) (Benjamini
346 and Hochberg, 1995), which accounts for the fact that the same hypotheses are iteratively tested multiple times. The corrected
347 p -values then determine whether a link between two actors is considered “causal”.

348 The causal effect is then calculated by linearly regressing each actor on its own set of causal parents. E.g., assuming that the
349 causal parents of $A_{t=0}$ are $P_A^n = \{A_{t=-1}, C_{t=-1}, D_{t=-2}\}$, then the following multilinear regression equation will be calculated:

350
$$A_{t=0} = \beta_A * A_{t=-1} + \beta_C * C_{t=-1} + \beta_D * D_{t=-2} + \xi_A \tag{4}$$

351 Where β_i is the causal effect of each parent x_i . With standardized actors, a β_B value of 0.5 corresponds to a change of 0.5
352 standard deviation (s.d.) of $A_{t=0}$ given a change of 1 s.d. of $B_{t=-1}$ (given that all other parents remain unaltered). In this work,
353 we use the PCMCi algorithm as coded in Tigramite, version 5.2, and we use the PCMCiplus function, which allows us to
354 calculate links also at lag 0. However, lag 0 links are not “directed”, which means that the direction of causality is not
355 determined. The Tigramite package is publicly available and can be found at this link <https://github.com/jakobrunge/tigramite>.
356 The causal relationships obtained with PCMCi are then plotted in a causal effect network (CEN). In a CEN, each actor is
357 represented by a node in the network, while lagged causal relationships are represented by directed arrows, showing the
358 direction of causality. The colour of the arrows (nodes) shows the strength of the causal effect, the β value (auto β value), while
359 the numbers on the arrows show the lag at which the causal link is detected. Finally, the causal effect can also be calculated
360 by applying the concept of causal inference, rather than causal discovery. When causal inference is applied, the causal links
361 are determined a priori (generally based on expert-knowledge of the analysed physical system) and then the causal effect is
362 calculated following the same multi-linear regression model described earlier in Eq. (4). A detailed description of the Tigramite
363 functions and parameters used can be found in Text S2 in the Supplementary Material.

364 Here, linear correlation analysis and probability-trend estimation were conducted for all datasets mentioned. The correlation
365 and causal inference analyses were performed for both SEAS5.1-03 and SEAS5.1-05, except for CENs. For causal discovery,
366 only SEAS5.1-03 was used, as the absence of March and April data in SEAS5.1-05 violates PCMCi algorithm requirements.
367 Therefore, we mainly present results for SEAS5.1-03 in the main manuscript, while SEAS5.1-05 is available in the
368 Supplementary Material.

369 **2.4 Bootstrapping and significance**

370 To ensure statistical significance in the seasonal forecast data (SEAS5.1 initialized in March, May, and June), we employed
371 bootstrapping. We resampled the original set of 25 ensemble members x 43 years, creating 10,000 new samples by randomly
372 selecting one of the 25 ensemble members for each year along the timeseries from 1981 to 2023. This resampled distribution
373 of 10,000 timeseries is illustrated in various figures. When a single value for SEAS5.1 is mentioned, it refers to the median of

Deleted: .

Deleted: ¶

Deleted: 3

Deleted: 7¶

Formatted: Font colour: Black

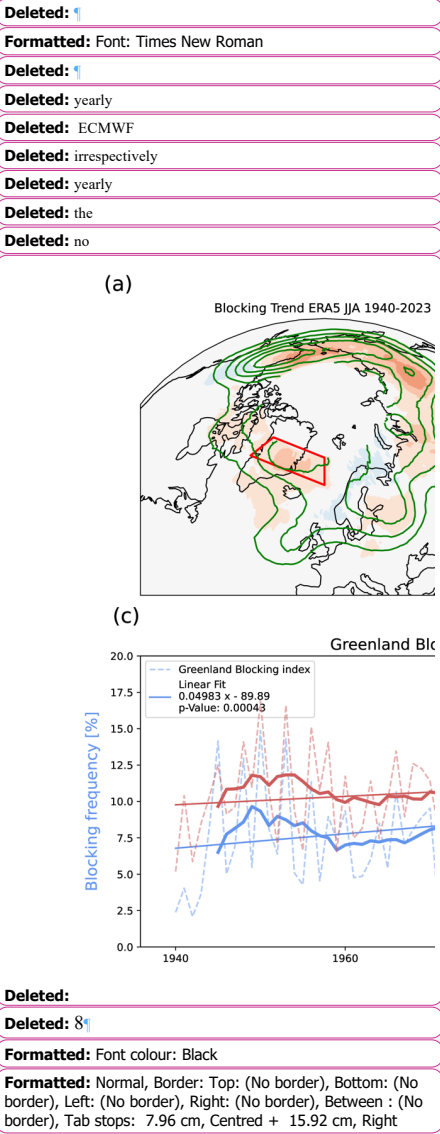
Formatted: Normal, Border: Top: (No border), Bottom: (No border), Left: (No border), Right: (No border), Between : (No border), Tab stops: 7.96 cm, Centred + 15.92 cm, Right

377 the bootstrapped distribution. For example, the correlation between two indices in SEAS5.1 is determined by calculating the
378 correlation values for all 10,000 timeseries and then taking the median of these values.

379 **3 Results**

380 **3.1 Greenland blocking indices and trends**

381 Greenland blocking in the summer season has increased its frequency in recent decades. Figure 1a and 1b show the grid-point
382 blocking frequency trends defined by the JJA seasonal averaged blocking index for ERA5 reanalysis for two different time
383 windows. However, notable differences emerge when focusing on different time windows: while in ERA5-40 the blocking
384 trend is positive in most of the Northern Hemisphere (Fig. 1a), the linear trend shows much larger spatial variability when
385 ERA5-81 is considered (Fig 1b), showing decrease in western Europe and western North America. Still, over the Greenland
386 Blocking region, highlighted by the red box in both panels, trends remain positive irrespective of the period considered.
387 The difference between the two trends may be related to the large interannual variability which characterizes blocking.
388 Blocking can easily achieve a frequency of 20% in certain summers and then show an almost negligible frequency in the
389 following year. This can be also seen in Figure 1c, where both the GBI (blue) and GGI (red) indices are reported, and the
390 year-to-year variability emerges evidently. A significant positive trend is observed in both cases (trends are significant at 99%
391 confidence level for both indices with a Mann-Kendall test). However, recent years are characterized by a reduction of blocking
392 from 2015 onward, which weakens the magnitude and the significance of the trend (Fig. S1 in the Supplementary Material).
393 It is important to notice that the seasonal averaged GGI and GBI indices are also highly correlated, showing a Pearson
394 correlation coefficient of $r = 0.8$. From a statistical point of view, this implies that the two indices are very similar and in the
395 rest of the manuscript we will employ GGI to perform the PCMCi analysis, which works best with non-binary indices.
396 Similar results can be obtained when using different blocking indices, as the HA16 and TY21 indices. Despite minor
397 differences inherently associated with their definitions, both indices display the same qualitative trends as seen in Fig. 1c (Fig.
398 S2-3 in the Supplementary Material).



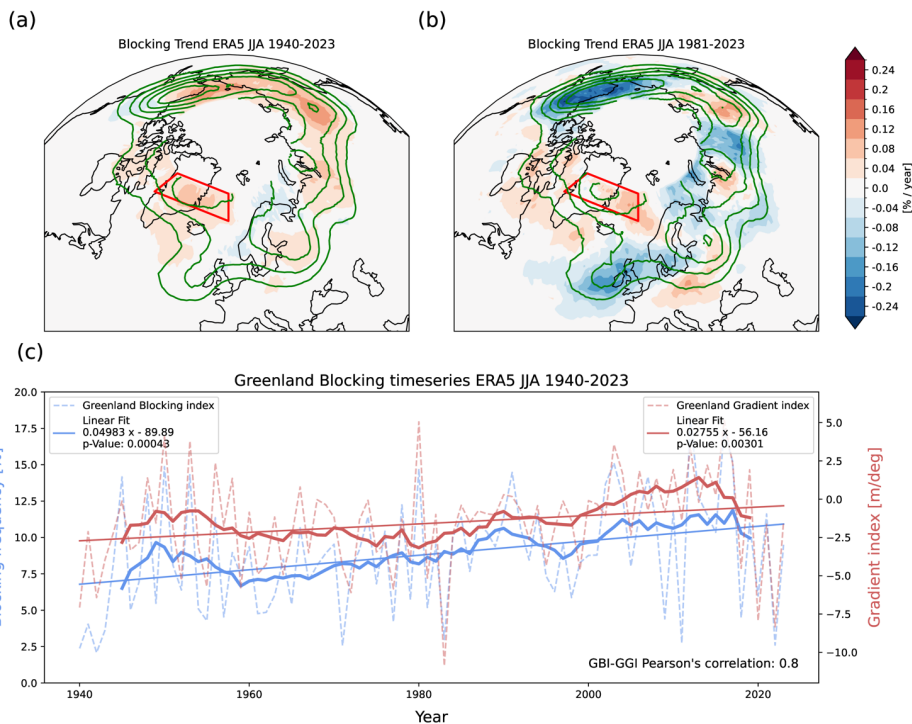


Figure 1: Greenland blocking index observed trends. Panel (a) shows blocking trend (shading) and blocking climatology (green contours) in boreal summer (JJA) over the Northern Hemisphere for ERA5-40. Contours are drawn every 3% blocked days. Panel (b): same as for Panel (a) but for ERA5-81. Panel (c) shows JJA Greenland Blocking Index (blue) and Greenland Gradient Index (red), measured as the averaged over the red box shown in panel (a) for ERA5-81. Dashed lines show the season average, bold lines the 10-year running mean and the thin solid lines the linear trend. Values for the trend and their *p*-values (estimated with a Mann-Kendall test) are shown in the legend for both indices.

Formatted: Font: *Italic*

Deleted: 9

Formatted: Font colour: Black

Formatted: Normal, Border: Top: (No border), Bottom: (No border), Left: (No border), Right: (No border), Between : (No border), Tab stops: 7.96 cm, Centred + 15.92 cm, Right

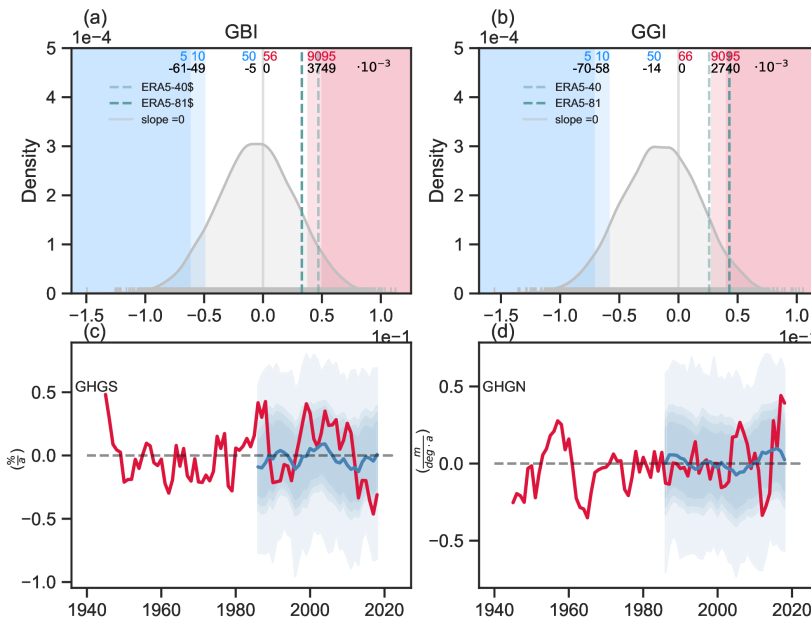
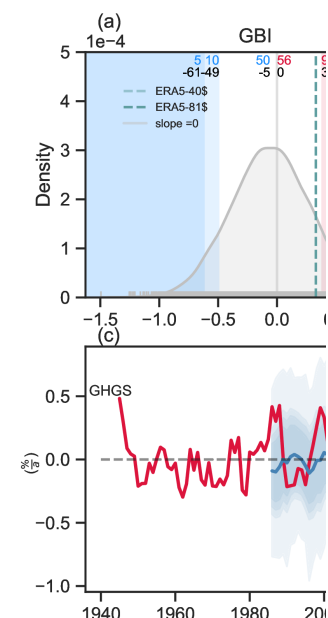


Figure 2: Greenland blocking and Greenland Gradient index trends in SEAS5.1-03 and ERA5. Panel (a) shows the Probability density function of JJA trends in GBI for the 10^4 different member permutations. Panel (b): same as for panel (a) but for the GGI index. Shaded vertical lines show values 5th, 10th, 90th and 95th percentiles. Percentiles are shown in blue (5th, 10th, 50th) and red (90th and 95th) with the corresponding trend values in black below. Percentile of the distribution of a slope of 0 is also given in red and indicated with the grey vertical line. Green dashed verticals indicate linear slope of ERA5-40 (light green) and ERA5-81 (solid green). Panel (c) shows the 11-year moving window trend of ERA5 (red) and the SEAS5.1-03 trend distribution (blue shadings) for the GBI. Panel (d) same as for panel (c) but for the GGI index. The dark blue line indicates the median 11-year running mean of the SEAS5.1-03 distribution.

Observed trends in GBI and GGI are shown in detail in Fig. 2. To compare the ERA5 trend with SEAS5.1-03 trends, we calculate a probability density function (PDF) of the 10^4 trends derived from our bootstrapped SEAS5.1-03 ensemble members (see Methods Section 2.4). In contrast to ERA5, the median values of the SEAS5.1-03 PDFs indicate negative trends for both GGI and GBI (Figs. 2a and 2b respectively). The ERA5-81 trend falls right below the 90th percentile for GBI (Fig. 2a) and between the 90th and the 95th percentiles for GGI (Fig. 2b). This suggests that albeit SEAS5.1-03 can reproduce the observed trends with certain specific combinations of ensemble members, the probability of doing so is relatively low (~5-10%). Using



Deleted:

Commented [1]: @joha.beckmann@googlemail.com we need to modify the c/d panel to remove GHGS/GHGN and replace with GBI/GGI (as well as the units on y-axis)

Deleted: combinations

Deleted:

Deleted: running

Deleted: 3a

Deleted: 3b

Deleted: -5

Deleted: 10%

Formatted: Font colour: Black

Formatted: Normal, Border: Top: (No border), Bottom: (No border), Left: (No border), Right: (No border), Between: (No border), Tab stops: 7.96 cm, Centred + 15.92 cm, Right

437 later initialization dates (SEAS5.1-05 and SEAS5.1-06) does not increase the likelihood of matching the observed trends (see
438 Fig. S4 in the Supplementary Material). We provide the same analysis using the GHGS and GHGN components of the
439 Greenland Blocking index (Fig. S5 in the Supplementary Material) and show that the probability of reproducing the observed
440 trend is slightly higher for GHGN, while it is very low for GHGS (below 2.5%), indicating that GHGS may be the primary
441 source of the low agreement between ERA5 and SEAS5.1 trends. We also check the trends obtained with the HA16 index,
442 which shows qualitatively similar results (see Fig. S6 in the Supplementary Material).

443 To investigate the multidecadal variability of the blocking trends, we run an 11-year moving window trend on the ERA5 and
444 SEAS5.1 timeseries (Figs. 2c and 2d). SEAS5.1 trends are shown both as the ensemble mean trend (blue solid line in Fig. 2c-
445 d), or as the distribution of trends obtained from each of the 10^4 realizations (blue shading in Fig. 2c-d). The timeseries of
446 ERA5 reveals that the short-term blocking trend (for both GBI and GGI) fluctuates between positive and negative values,
447 indicating a strong influence from climate variability on decadal timescale. Particularly in recent years, the moving window
448 trend shows remarkable negative trends, which explains the loss of significance for the GBI observed for the ERA5-81 trend
449 (Fig. S1). The ERA5 moving window trend lies in the ensemble of the bootstrapped SEAS5.1 ensemble, where the median
450 SEAS5.1 trend shows a switching of the sign as well but not always aligned with ERA5.

452 Next, we check the relationship between GGI and surface temperatures over the extended North Atlantic sector (Figs. 3a-b),
453 to quantify the relationship between high GGI indices and positive temperature anomalies over the Greenland ice sheet, in both
454 reanalysis and seasonal forecast. We calculate composites of T2m and Z500 fields during days for which GGI values are
455 greater than their JJA s.d. ($\text{GGI} > 1 \text{ s.d.}$) for both ERA5-81 (Fig. 3a) and SEAS5.1-03 (Fig. 3b) datasets. Z500 composites for
456 ERA5 show the expected ridge centred over eastern Greenland, which is paired with a trough to the south, centred west of the
457 British Isles (Fig. 3a). This north-south dipole pattern is also present with a similar shape, location and strength of the Z500
458 anomalies in the SEAS5.1-03 composite (Fig. 3b). Positive T2m anomalies are shown over Greenland for both ERA5 and
459 SEAS5.1-03, reaching values of +2.5K while over the Arctic Ocean and the North Atlantic weak negative anomalies are shown
460 -0.5K, shading in Figs. 3a-b). The difference between SEAS5.1-03 and ERA5 composites for both T2m and Z500 shows a
461 tendency of the model to have higher Z500 anomalies over Greenland and the North Atlantic and higher T2m anomalies over
462 Greenland and Northern Canada with respect to ERA5 (Figs. 3c-d).

463 The PDF showing the distribution of the GGI index is shown in Fig. 3e for ERA5-81 and Fig. 3f for SEAS5.1-03 and provides
464 a measure of the daily variability of the Z500 field over Greenland in summer. The JJA GGI mean value is -1.52 m for ERA5-
465 81 and -1.39 m for SEAS5.1-03, while the s.d. values are 10.1 m and 11.8 m respectively. Thus, the variance in SEAS5.1-03
466 is slightly overestimated with respect to ERA5-81. Note that GGI values are detrended and the anomalies are centred around
467 zero (as described in Section 2.1).

Deleted: S2

Deleted: S3

Deleted: running

Deleted: running mean

Deleted: running mean

Formatted: Font colour: Black

Deleted: .

Deleted: a

Deleted: , which resembles a negative North Atlantic Oscillation (NAO) phase (though shifted northwards),

Deleted: (-.

Moved (insertion) [3]

Deleted: 3c

Deleted: 3d

Moved up [3]: 3c-d).

Deleted: (Figs.

Deleted: 11

Formatted: Font colour: Black

Formatted: Normal, Border: Top: (No border), Bottom: (No border), Left: (No border), Right: (No border), Between : (No border), Tab stops: 7.96 cm, Centred + 15.92 cm, Right

483 High pressure systems over Greenland are associated with high temperature anomalies both in SEAS5.1 and ERA5 (Fig. 3a-
484 b). Temperature over Greenland is then calculated by spatially averaging T2m values over the box 67-81°N, 25-55°W, and the
485 corresponding index is named T2m-Greenland (T2m-G). The JJA climatological PDFs for T2m-G for ERA5 and SEAS5.1-
486 03 are shown in Figs. 3g and 3h respectively (orange shading in Figs. 3g-h). T2m-Greenland for SEAS5.1 has a comparable
487 mean value and slightly larger standard deviation than ERA5.
488 The effect of GGI on T2m is then quantified by calculating the T2m-G PDFs sub-selecting only days for which GGI > 1 s.d.
489 (shown are red lines in Figs. 3g-h). For ERA5-81, the T2m-G PDF strongly shifts towards higher T2m values for GGI > 1 s.d.,
490 with 85% of the values falling above the 50th quantile and 28% of the data exceed the climatological 90th quantile, thus showing
491 a 3-fold increase in the probability of extreme heat (Fig. 3g). Similarly, the SEAS5.1-03 T2m-G PDF for days where GGI > 1
492 s.d. also shows a strong shift towards higher T2m values, with 88% of the data falling above the 50th climatological quantile
493 and 35% of the data exceed the 90th climatological quantile, consistently showing a 3-fold increase in extreme T2m-G values
494 (Fig. 3h). Hence, high GGI values are generally related to higher than average T2m-G values both in ERA5-81 and SEAS5.1-
495 03, showing a good linkage between geopotential height anomalies and temperature anomalies in the seasonal forecast system.
496 However, the relationship to extreme T2m-G values is more marked in SEAS5.1-03.
497 The same Figures but for GGI SEAS5.1-05, for SEAS5.1-03 GHGS and GHGN, as well as for the HA16 index show consistent
498 results, even though for positive GHGN values the sign of the Z500 and T2m anomalies is inverted (see Supplementary
499 Material, from S7 to S10).

Deleted: Figs

Deleted: ,

Deleted: 3e

Deleted: 3f

Deleted: 3e-f

Deleted: of 265.7 K (264.8 K) for ERA5-81 (SEAS5.1-03)

Deleted: a s.d. of 2.1 K (3.1 K) for ERA5-81 (SEAS5.1-03).

Deleted: 3e-f

Deleted: 3e

Deleted: 33

Deleted: 3f

Deleted: .

Deleted: and

Deleted: Figs. S4, S5 and S6 respectively

Deleted: 12

Formatted: Font colour: Black

Formatted: Normal, Border: Top: (No border), Bottom: (No border), Left: (No border), Right: (No border), Between : (No border), Tab stops: 7.96 cm, Centred + 15.92 cm, Right

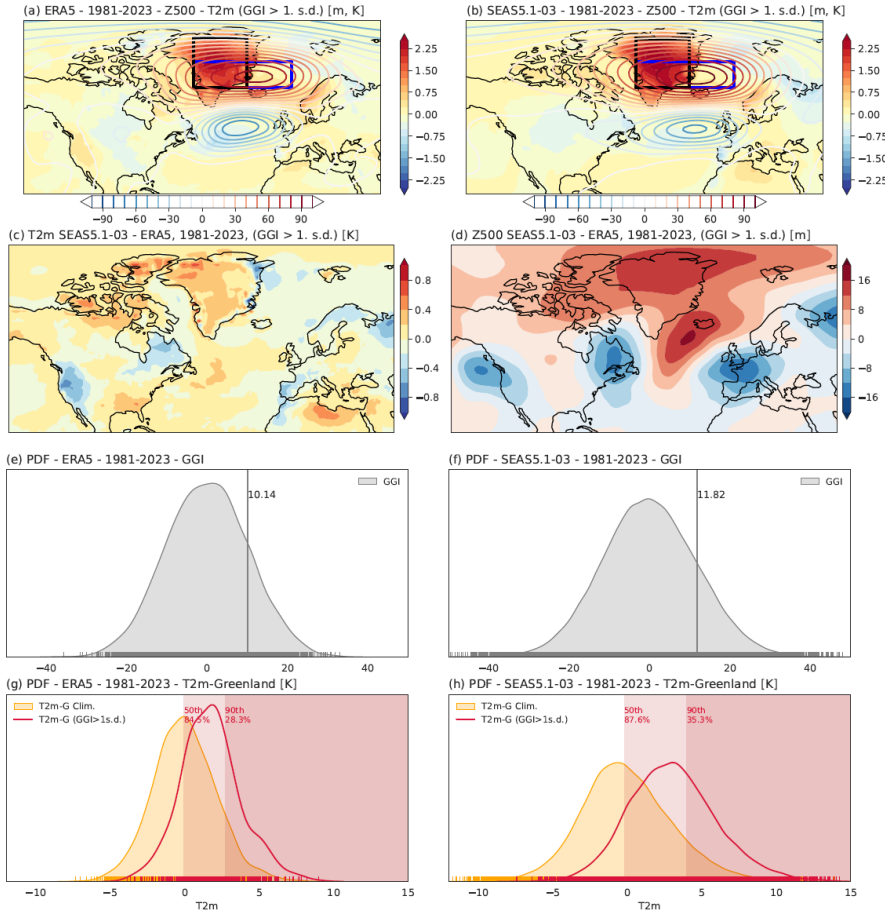
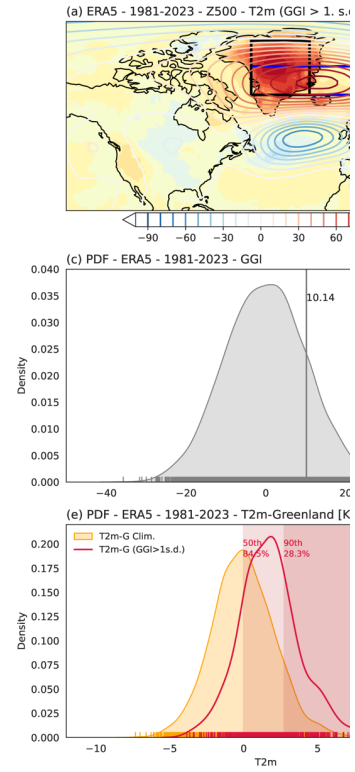


Figure 3. GBI and extreme temperatures over Greenland. Panel (a): composite of JJA Z500 (contours) and T2m (shaded) anomalies for (daily) time steps with GGI > 1 s.d. for ERA5-81. Panel (b): Same as panel (a) but for the SEAS5.1-03 dataset (25 ensemble members each year). Panel (c): difference between the SEAS5.1-03 and the ERA5 T2m composites shown in Panels (a)-(b). Panel (d): Same as for Panel (c) but for the Z500 field. Panel (e): probability density function (PDF) for the Greenland gradient index (GGI) daily climatology for ERA5-81. Panel (f): Same as for Panel (e) but for SEAS5.1-03 dataset. Panel (g): PDF for the T2m-Greenland (T2m-G) daily climatology (orange) and sub-selected days with GGI > 1 s.d. (red) for ERA5-81. Red shading in the plot highlights the position of the climatological 50th and 90th percentiles, while the numbers below the percentiles show the percentage of T2m-G which is above the climatological percentile in the sub-selected PDF. Panel (h): Same as for Panel (g) but for SEAS5.1-03.



Deleted:

Deleted: Panel (c)

Deleted: d

Deleted: c

Deleted: c

Deleted: Panel (f): Same as for Panel (2)

Deleted: 13

Formatted: Font colour: Black

Formatted: Normal, Border: Top: (No border), Bottom: (No border), Left: (No border), Right: (No border), Between : (No border), Tab stops: 7.96 cm, Centred + 15.92 cm, Right

529 3.2 Potential drivers of Greenland blocking at monthly time scales

530 We identify four monthly potential drivers ~~for~~ GGI variability based on hypothesized mechanisms described in ~~Section 1~~.
531 These potential drivers are: (i) T2m over the Arctic circle (T2m-Arctic, an indicator for Arctic ~~warming~~), (ii) snow cover over
532 northern North America (Snow-NAm), (iii) MSLP over the eastern ~~North America~~ (MSLP-NAm, following the mechanism
533 identified by Preece et al 2023) and (iv) the Atlantic ~~Multidecadal Variability~~ (AMV) index. The spatial domain and acronym
534 of each index is reported in Table 1, ~~and resulting analysis is presented in Figure 4~~.

535
536 Figures 4a,e show the composites of T2m fields over months where the T2m-Arctic index is above ~~1~~ s.d. (T2m-Arctic > 1 s.d.)
537 for ERA5-81 and SEAS5.1-03 respectively. As expected, high surface temperature anomalies up to 2°C are seen over the polar
538 cap (latitude > 60°N) over land, while over the Arctic Ocean weak negative anomalies are detected. This result confirms the
539 tendency of high-latitude land to warm up more strongly in summer, compared to the Arctic Ocean (Di Capua et al., 2021).
540 Over mid-latitude and tropical land-ocean surfaces, T2m anomalies tend to be positive both in ERA5-81 and SEAS5.1-03.
541 However, in SEAS5.1-03 T2m anomalies are much weaker outside the Arctic circle (Fig. 4e), while in ERA5 strong warming
542 is also detected over Europe, western Russia, the Middle East, southwestern ~~United States~~ and mid-latitude North Pacific (Fig.
543 4e). This discrepancy between ERA5 and SEAS5.1-03 may be explained by the different size of the two sub-samples: while
544 ERA5-81 contains a total of 3*43 = 129 ~~summer~~ months, SEAS5.1-03 contains 25 times more. Since 1940, T2m-Arctic has
545 shown a significant positive trend that has doubled in the time frame from 1981-2023 (Figure ~~S11~~ in the Supplementary
546 Material). The 11-year ~~moving window trend~~ (Fig. 4i) shows that T2m-Arctic fluctuates between positive and negative values
547 since 1940 but has stayed positive since around 2000. The majority of the bootstrapped SEAS5.1-03 experiences this continued
548 positive trend as well indicated by the blue-shaded ensemble distribution in Fig. 4i and the SEAS5.1-03 median values in thick
549 blue, showing that the polar cap warming is well captured by the model.

Index	Acronym	Spatial domain
Greenland blocking index	GBI	55°W-0°, 67°N-75°N
Greenland gradient index	GGI	55°W-0°, 67°N-75°N
Geopotential height gradient South	GHGS	55°W-0°, 67°N-75°N
Geopotential height gradient North	GHGN	55°W-0°, 67°N-75°N
Atlantic multidecadal variability	AMV	80°W-0°, 0°-60°N
Snow cover over North America	Snow-NAm	70°-135°W, 40°-75°N
Mean sea level pressure over North America	MSLP-NAm	70°-105°E, 30°-50°N
Arctic 2m temperature	T2m-Arctic	180°W-180°E, 60°-90°N

550 Table1. Summary of indices with their corresponding acronyms and spatial domains.
551

Deleted: of
Deleted: the Introduction
Deleted: amplification
Deleted: US
Deleted: multidecadal variability
Deleted: .

Deleted: its own

Deleted: US

Deleted: is summer

Deleted: S7

Deleted: running mean

Formatted Table

Deleted: Artic

Deleted: 14

Formatted: Font colour: Black

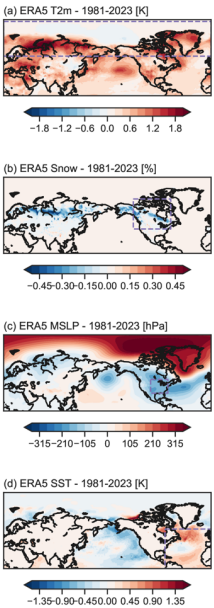
Formatted: Normal, Border: Top: (No border), Bottom: (No border), Left: (No border), Right: (No border), Between : (No border), Tab stops: 7.96 cm, Centred + 15.92 cm, Right

564 Composites for Snow over North America during months with Snow-NAM < 1 s.d. (May only) are shown in Fig. 4b,f for
565 ERA5-81 and SEAS5.1-03 respectively. ERA5-81 shows lower than average Snow anomalies over Alaska, at the border
566 between the [United States](#) and Canada, and in Siberia (Fig. 4b), while SEAS5.1-03 only shows negative Snow anomalies over
567 North America (Fig. 4f). Since 1960, the 11-year [moving window](#) trend of Snow (Fig. 4j) has generally shown negative values,
568 with only brief and minor episodes of positive values. In recent years, there has been a positive trend in the ERA5 Snow data;
569 however, the overall snow cover remains below the 1940-2023 mean (Fig. [S11](#) in the Supplementary Material). Meanwhile,
570 the SEAS5.1-03 ensemble exhibits significant fluctuations between positive and negative 11-year [moving window](#) trends (Fig.
571 4j), suggesting that snow cover may not be accurately captured in SEAS5.1.
572 Composites for MSLP fields during months with MSLP-NAM < 1 s.d. are shown in Figs. 4c and 4g for ERA5-81 and SEAS5.1-
573 03 respectively. Months with low MSLP-NAM are associated with low MSLP anomalies over [North America](#), the mid-latitude
574 North Atlantic both for ERA5-81 and SEAS5.1-03. High MSLP anomalies are shown over the Arctic circle and Greenland
575 (Figs. 4c-g). The 11-year [moving window](#) trend of MSLP-NAM has shown strong fluctuations between positive and negative
576 trends throughout the entire period from 1940 to 2023 (Fig. 4k). These fluctuations are well captured by the bootstrapped
577 SEAS5.1-03 ensemble since 1981. Over the whole timeseries, we can see a statistically significant negative trend in MSLP-
578 Nam for ERA5, with a doubling of the negative slope since 1981 (Fig. [S11](#) in the Supplementary Material).
579 Finally, composites for SST anomalies during months with AMV > 1 s.d. are shown in Fig. 4d,h for ERA5-81 and SEAS5.1-
580 03 respectively (the [AMV](#) is calculated following Zhang et al (2019), see Text S3 in Supplementary). Positive SST anomalies
581 are found over high-latitude North Atlantic, west of the European and African coasts and over the tropical North Atlantic,
582 while cold anomalies are shown over mid-latitude eastern North Atlantic (Figs. 4d,h). Cold anomalies are also seen over the
583 western North Pacific for both ERA5-81 and SEAS5.1-03, while warm anomalies over mid-latitude North Pacific are clearly
584 seen only in SEAS5.1-03 (Fig. 4h). The AMV exhibits strong fluctuations in both the sign and values of the 11-year [moving](#)
585 [window](#) trend, which are well represented by the bootstrapped SEAS5.1-03 ensemble (Fig. 4l).
586 [Note that both AMV and Snow-NAM SEAS5.1 indices are more tightly constrained than other indices. This is due to the fact](#)
587 [that SST or snow cover fields are characterized by larger inertia and have a slower variability than atmospheric fields, such as](#)
588 [T2m or Z500. The next will assess the relationships among these indices and GBI.](#)

Deleted: US...nited States and Canada, and in Siberia (Fig. 4b), while SEAS5.1-03 only shows negative Snow anomalies over North America (Fig. 4f). Since 1960, the 11-year running mean...oving window trend of Snow (Fig. 4j) has generally shown negative values, with only brief and minor episodes of positive values. In recent years, there has been a positive trend in the ERA5 Snow data; however, the overall snow cover remains below the 1940-2023 mean (Fig. [S11](#) in the Supplementary Material). Meanwhile, the SEAS5.1-03 ensemble exhibits significant fluctuations between positive and negative 11-year [moving window](#) trends (Fig. 4j), suggesting that snow cover may not be accurately captured in SEAS5.1. [6]

Deleted: the US, Canada...orth America, the mid-latitude North Atlantic both for ERA5-81 and SEAS5.1-03. High MSLP anomalies are shown over the Arctic circle and Greenland (Figs. 4c-g). The 11-year running mean...oving window trend of MSLP-NAM has shown strong fluctuations between positive and negative trends throughout the entire period from 1940 to 2023 (Fig. 4k). These fluctuations are well captured by the bootstrapped SEAS5.1-03 ensemble since 1981. Over the whole timeseries, we can see a statistically significant negative trend in MSLP-Nam for ERA5, with a doubling of the negative slope since 1981 (Fig. [S11](#) in the Supplementary Material). [7]

Deleted: AVM...MV is calculated following Zhang et al (2019), see Text S3 in Supplementary). Positive SST anomalies are found over high-latitude North Atlantic, west of the European and African coasts and over the tropical North Atlantic, while cold anomalies are shown over mid-latitude eastern North Atlantic (Figs. 4d,h). Cold anomalies are also seen over the western North Pacific for both ERA5-81 and SEAS5.1-03, while warm anomalies over mid-l [8]



Deleted:
Commented [2]: this section perhaps misses a conclusion, What do you think? @giorgia.dicapua@gmail.com @joha.beckmann@googlemail.com

Deleted: 15
Formatted: Font colour: Black

Formatted: Normal, Border: Top: (No border), Bottom: (No border), Left: (No border), Right: (No border), Between : (No border), Tab stops: 7.96 cm, Centred + 15.92 cm, Right

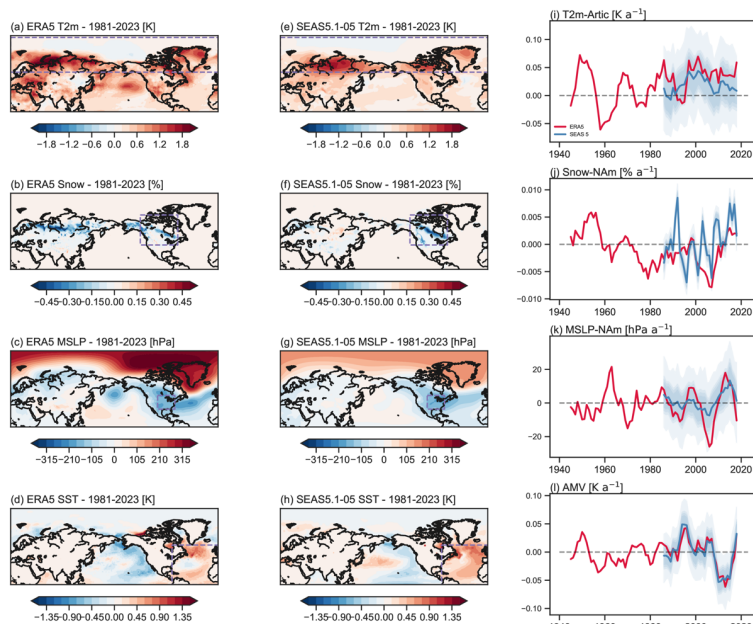


Figure 4. Composites and 11-year moving window trend of monthly indices. Panel (a) shows the composites of JJA T2m fields for months with T2m-Arctic > 1 s.d. for ERA5-81. Panel (b) same as for Panel (a) but for snow coverage in May during months with Snow-NAm < 1 s.d.. Panel (c) as for Panel (a) but for MSLP fields during months with MSLP-NAm < 1 s.d.. Panel (d) as for Panel (a) but for SST fields during months with AMV > 1 s.d.. Panels (e)-(h) same as for panels (a)-(d) but for SEAS5.1-03. For each panel, the grey dashed box in (a-h) indicates the area from which the monthly indices (T2m-Arctic, Snow-NAm, MSLP-NAm, AMV) were derived. Panels (i) illustrates the 11-year moving window trend of T2m-Arctic for ERA5 (red) and the SEAS5.1-03 distribution of 10⁴ timeseries in blue shades. Panels (j)-(l) same as for panel (i) but for Snow-NAm, MSLP-NAm, and AMV. The thick blue line indicates the median value of the total distribution. The grey dashed line indicates the moving window trend of ~0.

Deleted: running mean

Deleted: Panels

Deleted: Snow fields

Commented [3]: is the caption or the title wrong here? Are we using SEAS5.1-03 or SEAS5.1-05 for the figure?
@joha.beckmann@googlemail.com
@giorgia.dicapua@gmail.com

Commented [4R3]: it should be SEAS5.1, possibly the titles in the figure are wrong

Commented [5R3]: do you mean SEAS5.1-03?

Deleted: >

Deleted: The

Commented [6]: would it be possible to use another color? The box is almost impossible to see
@joha.beckmann@googlemail.com

Deleted: running mean

Deleted: running mean

Deleted: 16

Formatted: Font colour: Black

Formatted: Normal, Border: Top: (No border), Bottom: (No border), Left: (No border), Right: (No border), Between : (No border), Tab stops: 7.96 cm, Centred + 15.92 cm, Right

668 3.3 Relationship among climate drivers and blocking indices

669 Following the characterization of the potential GBI drivers from Section 3.2, we would like to assess their actual relationship
670 with Greenland Blocking in both ERA5 and SEAS5.1. Indeed, one of the goals of this study is to test the Preece et al. (2023)
671 hypothesis, hereafter referred to as “Preece23”, which suggests that Arctic warming may induce early snow cover depletion in
672 May over North America, generating a low-pressure anomaly, which in turn could act as a waveguide, leading to blocking
673 over Greenland. Additionally, we aim to assess whether summer Greenland blocking is influenced by the AMV and evaluate
674 SEAS5.1’s ability to replicate the observed correlations. To investigate the relationship between various blocking indices (GBI,
675 GGI, GHGS, GHGN) and key climate drivers (AMV, T2M-Arctic, Snow-NAm, MSLP-NAm, whose properties has been
676 assessed in the previous section), we calculate a correlation heatmap using detrended variables from ERA5-40, ERA5-81, and
677 SEAS5.1-03 (Fig. 5). All time series are linearly detrended, except for ERA5-40 T2M-Arctic, which is detrended using a
678 polynomial function due to its non-linear trend.

679 We first focus on the GBI index in relation to Preece23’s hypothesis. In ERA5-81, positive (lag 0) correlations are found
680 between both T2M-Arctic, MSLP-NAm and GBI ($r \sim 0.3$), while Snow-NAm (taken in May) shows a negative correlation
681 with GBI ($r \sim -0.2$). Conversely, the correlation between AMV and GBI is $r \sim 0$. However, only the correlation between T2M-
682 Arctic and GBI is statistically significant ($p < 0.05$), supporting only the first part of the hypothesis linking Arctic warming to
683 enhanced GBI (Fig. 5b).

684 When comparing the original blocking index (GBI) to the derived GGI, the correlation values are qualitatively similar with
685 some differences: the correlation between MSLP-NAm, T2m-Arctic and GGI decrease and are not significant for ERA5-81,
686 while the correlation with Snow-NAm increases to a significant $r \sim 0.35$ (Fig. 5b). The correlation between GHGS and the
687 precursors indices is qualitatively similar to that of GGI, with the difference that GHGS also shows a negative ($r \sim -0.3$) and
688 significant correlation with MSLP-NAm. Interestingly, $\text{GHGS} > 0$ is a requirement to have blocking over Greenland; however,
689 the fact that this negative correlation does not show up for GBI and GGI may be because the correlation between GHGN and
690 MSLP-NAm is also negative ($r \sim -0.5$), weakening the possible connection with blocking.

691 Indeed, GBI requires both GHGS and GHGN conditions to be met simultaneously, while GGI is a linear combination of the
692 two. Thus, negative MSLP anomalies can lead to positive pressure anomalies over Greenland, which promote blocking
693 ($\text{GHGS} > 0$), but also negative pressure anomalies over eastern Greenland ($\text{GHGN} > 0$), reducing the likelihood of blocking. As
694 a result, the effects cancel out in GGI, leading to near-zero correlations with MSLP-NAm. Thus, disentangling the blocking
695 indices into GHGS and GHGN reveals more details of the complex relationship between MSLP-NAm and Greenland blocking.

696

697 Extending the analysis to ERA5-40 generally results in weaker and less significant correlations, although qualitatively the sign
698 of the correlation is consistent (Fig. 5a). Notably, the correlation between Snow-NAm, MSLP-NAm and GHGS and between
699 Snow-NAm and GHGN are significant ($r \sim -0.2$, 0.3 , Fig. 5a). This suggests that the proposed Preece23 mechanism may not
700 hold consistently over the complete available historical period. Two interpretations are possible: (i) Arctic warming may have

Deleted: One

Deleted: amplification (AA)

Moved down [4]: 5b).

Deleted: The

Deleted: These results support the first part of the hypothesis regarding the relationship between AA, decreased snow cover and enhanced GBI, but not the relationship between a low-pressure anomaly over North America and increased GBI (Fig.

Deleted:

Moved (insertion) [4]

Deleted:).

Deleted: $r \sim 0.35$ and is

Deleted: Figure S5 reveals that

Deleted: leads

Deleted: the gradients reversal with a high-pressure system

Deleted: , which could favour blocking. However

Formatted: Font colour: Auto

Formatted: Font colour: Auto

Formatted: Font colour: Auto

Formatted: Font colour: Auto

Deleted: GBI

Deleted:).

Formatted: Font colour: Auto

Deleted: Notably, GHGN must be negative to contribute to blocking. ...

Deleted: -

Deleted: longer

Deleted: amplification

Deleted: 17

Formatted: Font colour: Black

Formatted: Normal, Border: Top: (No border), Bottom: (No border), Left: (No border), Right: (No border), Between : (No border), Tab stops: 7.96 cm, Centred + 15.92 cm, Right

723 become more dominant only in recent decades and (ii) the stronger signal observed in ERA5-81 may result from sampling of
724 internal variability.

725 When the correlation between the potential drivers among each other is considered, both ERA-40 and ERA-81 generally show
726 consistent qualitative results (Figs. 5a and 5b respectively). Both AMV and T2m-Arctic exhibit negative correlations with
727 MSLP-NAm and Snow-NAm ($r \sim -0.1-0.4$), while T2m-Arctic and AMV are positively correlated ($r \sim 0.3$). Snow-NAm and
728 MSLP-NAm are also positively correlated ($r \sim 0.1-0.4$). However, the strength of these correlations varies between the periods,
729 with stronger correlations found in ERA5-81 (Fig. 5b). In general, no direct correlation is found between AMV and the
730 blocking indices, indicating that AMV's influence on blocking may be indirect, primarily acting through MSLP-NAm.

731

732 Finally, we assess whether SEAS5.1-03 can replicate the observed correlations (Fig. 5c). SEAS5.1-03 generally weaker
733 correlations, which are somehow expected given the usual small signal-to-noise ratio of prediction systems typical over the
734 North Atlantic sector (Scaife and Smith, 2018). The correlation values in Fig. 5c represents the median of the distribution for
735 each pair of time series, with standard deviations shown in Fig. S12 in the Supplementary Material. Despite this difference,
736 SEAS5.1-03 replicates key patterns, especially the correlations among AMV, T2M-Arctic, and Snow-NAm. The positive
737 correlation between T2m-Arctic and the blocking indices is weaker ($r \sim 0.1-0.2$) but consistent with what is shown in ERA5-
738 81. In contrast, SEAS5.1-03 struggles to capture correlations between Snow-NAm, MSLP-NAm, and the blocking indices,
739 except for a weak negative correlation between MSLP-NAm and GHGS ($r \sim -0.2$). As snow cover in SEAS5.1-03 is derived
740 from climate model variables rather than observational data, we test whether a later initialization in SEAS5.1 (closer to
741 observed snow cover) could improve these correlations (see Fig. S12 in the Supplementary Material). We examine SEAS5.1-
742 05, which uses ERA5.1 snow cover initialized on May 1, and SEAS5.1-06, which allows for snow cover over the entire month
743 of May as calculated in ERA5-81. While this later initialization strengthens correlations among the climate drivers,
744 unfortunately it does not improve their relationship with the blocking indices.

745 Thus, in ERA5 our findings generally support the first part of Preece23's hypothesis, showing that T2M-Arctic and May snow
746 cover may influence MSLP over North America, which in turn favours pressure highs over Greenland ($GHGS > 0$). However,
747 this does not consistently lead to blocking, as MSLP also contributes to $GHGN > 0$, reducing the likelihood of blocking. The
748 AMV appears to have a moderate influence on MSLP and Arctic temperature, potentially affecting blocking indirectly. While
749 SEAS5.1-03 to SEAS5.1-06 captures relationships among climate drivers similar to those seen in observational data, they fail
750 to replicate the full extent of snow cover's role in blocking indices, particularly in relation to MSLP. This suggests a potential
751 misrepresentation of the driver-blocking interactions in the model, or missing elements in snow field initialization. Using the
752 HA16 index leads to qualitatively similar results for both ERA5 and SEAS5.1 (see Fig. S13 in the Supplementary Material),
753 even though, as expected, some stronger relationship emerges for ERA5. Further analysis in the next Section will explore
754 causal relationships between these drivers and blocking indices.

755

Deleted: Due to the large number of bootstrapped time series,

Deleted: shows lower signal-to-noise ratios, leading to

Formatted: Font colour: Auto

Deleted: .

Deleted: S8

Deleted: S8

Deleted: an

Deleted: .

Commented [7]: @joha.beckmann@googlemail.com
@giorgia.dicapua@gmail.com added this comment here since
number are somehow larger for Hanna

Deleted: .

Deleted: 18

Formatted: Font colour: Black

Formatted: Normal, Border: Top: (No border), Bottom: (No
border), Left: (No border), Right: (No border), Between : (No
border), Tab stops: 7.96 cm, Centred + 15.92 cm, Right

764
765
766
767
768
769
770
771

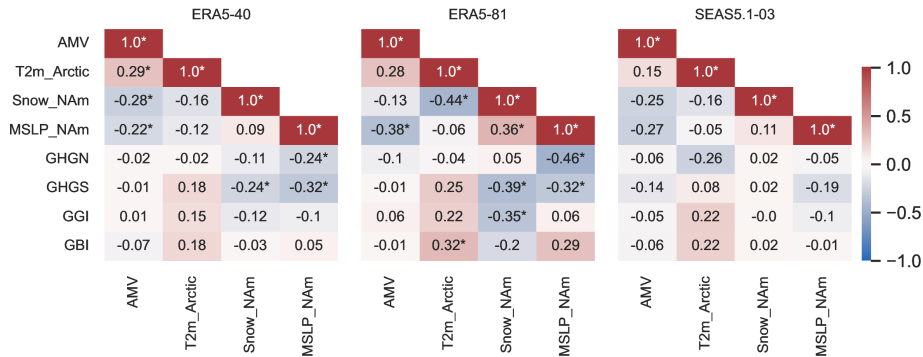


Figure 5. Summer correlation heat maps. Panel (a) shows the correlation of the different blocking indices (GBI, GGI, GHGS, GHGN) and the four identified potential monthly drivers (AMV, T2M-Arctic, Snow-NAm, MSLP-NAm) in ERA5-40 for the summer season. Panel (b) same as panel (a) but for ERA5-81. Panel (c) same for panel (b) but for SEAS5.1-03. All data were linearly detrended except for T2M-Arctic in ERA5-40 which was detrended using a polynomial fit. Statistically significant values at $p < 0.05$ are marked with an asterisk. The SEAS5.1-03 correlation values represent the median correlations from the 10^4 bootstrapped samples. The correlations were analysed for summer (JJA averaged) for all variables, while snow cover data were taken from the monthly mean in May.

3.4 Causal relationship in ERA5 and SEAS5.1

To disentangle spurious correlations from causal relationships, we now apply PCMCI to detect the causal links between GGI and its potential drivers. First, we apply PCMCI to build a causal effect network (CEN) for monthly GGI, Snow-NAm, T2m-Arctic, MSLP-NAm and AMV. We use $\text{lag}_{\text{max}} = -2$ for ERA5-81 and $\text{lag}_{\text{max}} = -1$ for SEAS5.1-03 (this is necessary not to violate PCMCI requirements, see Methods Section 2.3), while lag_{min} is set to 0 for both ERA5-81 and SEAS5.1-03. Note that, given the shortness of the time series, we do not apply the FDR correction to ERA5-81, which would result in too few significant causal links. Thus, we use the obtained CENs not to make final statements about causal relationships, but rather to get a first reasonable estimate of the potential causal links and to provide a first comparison between ERA5-81 and SEAS5.1-03. The ERA5-81 CEN (Fig. 6a) shows two incoming causal links towards GGI at lag -2 , one negative ($\beta = -0.15$) from Snow-NAm and one positive ($\beta = 0.15$) from T2m-Arctic. A negative undirected link (lag 0) between AMV and GGI is also present ($\beta = -0.15$). These links mean that lower than average Snow over North America during April-May-June (AMJ) is followed by higher than average GGI values in JJA. Similarly, though with opposite signs, higher than average T2m over the Arctic

Deleted:

Deleted: 19

Formatted: Font colour: Black

Formatted: Normal, Border: Top: (No border), Bottom: (No border), Left: (No border), Right: (No border), Between : (No border), Tab stops: 7.96 cm, Centred + 15.92 cm, Right

circle in AMJ are followed by higher than average GGI values in JJA. Thus, these links would support Preece23’s hypothesis that early snow cover depletion over North America can lead to more blocking. Similarly, the link from T2m-Arctic hints to the potential relevance of Arctic [warming](#) for blocking. The undirected link between AMV and GGI shows that lower than average AMV values in JJA correspond to higher than average GGI values in the same months. MSLP-NAM shows only one incoming positive ($\beta = 0.15$) link from Snow-NAM at lag -2 , meaning that higher than average Snow-NAM values in AMJ are followed by higher MSLP anomalies over [eastern North America](#), also in [keeping](#) with Preece23. Snow-NAM shows three incoming links: one positive link from MSLP-NAM at lag -1 ($\beta = 0.15$), and two negative links, one from T2m-Arctic at lag -1 ($\beta = -0.3$) and one from AMV at lag -2 from AMV ($\beta = -0.15$). Thus, higher than average Arctic temperatures and SST over the North Atlantic are both followed by lower than average Snow anomalies in the following months, while higher than average MSLP-NAM anomalies lead to higher Snow anomalies. Thus, Arctic warming has the potential to contribute to snow depletion and in turn to increased blocking. T2m-Arctic shows only one incoming negative link at lag -2 ($\beta = 0.15$) from Snow-NAM. Finally, AMV also shows only one positive incoming link at lag -1 from T2m-Arctic ($\beta = 0.15$).

The same CEN but for SEAS5.1-03 is shown in Fig. 6b. In general, a similar network structure is shown, with the following differences: the GGI is connected to T2m-Arctic via a positive undirected link (lag 0, $\beta = 0.25$), to MSLP-NAM via a negative undirected link (lag 0, $\beta = -0.15$) and to AMV by a negative undirected link (lag 0, $\beta = -0.1$). A direct link from Snow-NAM is not present in SEAS5.1-03. The AMV shows one additional undirected link with MSLP-NAM (lag 0, $\beta = -0.1$) and two negative incoming links at lag -1 from MSLP-NAM ($\beta = -0.1$) and GGI ($\beta = -0.1$). Two undirected links are also shown between MSLP-NAM and Snow (lag 0, $\beta = 0.1$) and between the latter and T2m-Arctic (lag 0, $\beta = -0.1$). These results show that ERA5-81 and SEAS5.1-03 generally agree on the causal links found among MSLP-NAM, Snow-NAM and T2m-Arctic. However, the direct causal link from Snow-NAM towards GGI is missing, while the undirected link from MSLP-NAM appears. Note that ERA5-81 and SEAS5.1-03 CEN are not one-to-one comparable, because (i) the maximum lag used is different, (ii) the length of the two time series is different and (iii) a different set of causal precursors will by construction lead to different β -values.

In general, similar causal links are also detected when GHGS, GHGN and the HA16 index are analyzed (Figs. S14-15 in Supplementary Material). For ERA5-81, most links are consistent with what shown in Fig. 6a, with the following differences: (i) AMV and Snow-NAM are linked by a two-way negative causal link (Figs. S14a,b), (ii) the link from T2m-Arctic towards GHGS is missing (Fig. S14a) and (iii) MSLP-NAM shows a direct link towards both GHGS and GHGN (Figs. S14a,b). For SEAS5.1-03, again most links are consistent with what shown in Fig. 6b, with the following differences: (i) no direct link is found between MSLP-NAM and GHGN (Fig. S14d) and (ii) GHGS shows two additionally outgoing links towards T2m-Arctic and AMV (Fig. S14c). Note that GHGN links should have an opposite sign with respect to those shown for GHGS in order to have the same effect on GGI. E.g. a positive (negative) influence of T2m-Arctic on GHGS (GHGN) has a joint positive effect on GGI. In contrast, the negative effect of MSLP-NAM on both GHGS and GHGN (Figs. S14a-b) cancels out when GGI is considered (Fig. 6a) meaning we do not find the proposed connection between the wave source (MLSP-NAM) and the blocking (GGI, Fig. 6a) suggested by Preece23. However, given the direct link from snow cover to GHGS, but not to GHGN,

Deleted: amplification

Deleted: western US

Deleted: keep

Deleted:

Deleted: and

Deleted: Fig. S9

Deleted: S9a

Deleted: S9a

Deleted: S9a

Deleted: S9d

Deleted: S9c

Deleted: S9a

Deleted: 20

Formatted: Font colour: Black

Formatted: Normal, Border: Top: (No border), Bottom: (No border), Left: (No border), Right: (No border), Between : (No border), Tab stops: 7.96 cm, Centred + 15.92 cm, Right

831 this relationship extends to GGI, supporting the hypothesis that early snow cover depletion in May might influence blocking
832 patterns. Although the direct association between the AMV and the blocking gradients is not observed, an indirect influence
833 is suggested through a connection with MSLP-NAm, indicating at least some level of natural variability affecting the blocking
834 indices GHGS and GHGN.
835 Thus, in general, the proposed chain of causality supports the idea that all four potential drivers influence, directly or indirectly,
836 blocking over Greenland. In keeping with Preece23, higher Arctic temperatures are linked to snow cover depletion, which is
837 in turn linked to negative MSLP anomalies over North America. While it is unclear whether these negative anomalies can lead
838 to blocking, their influence on the meridional gradients is apparent. A direct link from snow cover towards GGI is only found
839 in ERA5-81, while both model and reanalysis show a link to Arctic temperatures. The Atlantic multidecadal sea surface
840 temperature variability is also negatively affecting blocking over Greenland and indirectly GHGS and GHGN, supporting the
841 hypothesis that natural variability also plays a role.

842
843

Deleted: keep

844
845
846
847
848

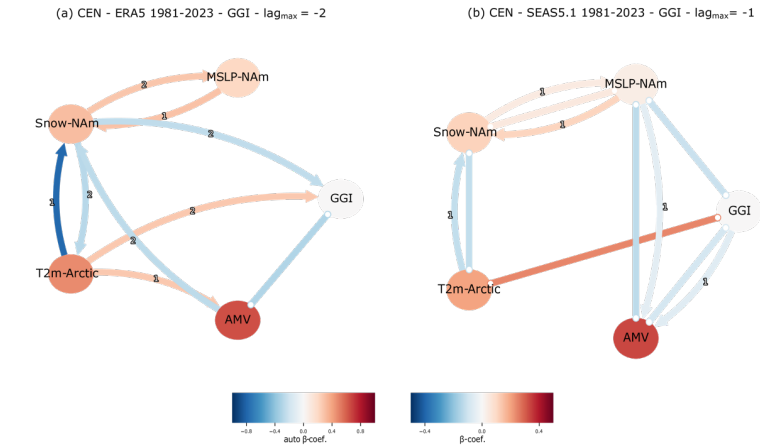
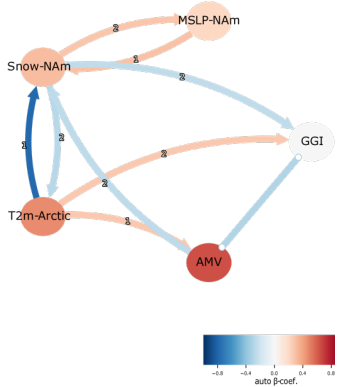


Figure 6. Causal effect networks for ERA5 and SEAS5.1-03. Panel (a): CEN with MSLP-NAm, Snow-NAm, T2m-Arctic, AMV and GGI for ERA5-81 and $\alpha = 0.05$ (no FDR applied, see Methods Section 2.3). Panel (b): same as for Panel (a) but for SEAS5.1-03 and with FDR correction applied. In each CEN, actors are represented by a node in the network, while lagged causal relationships are represented by directed arrows, showing the direction of causality. Lag 0 links are shown as straight arrows without an edge. The colour of the arrows

(a) CEN - ERA5 1981-2023 - GGI - lag_max = -2



Deleted:

Deleted: 21

Formatted: Font colour: Black

Formatted: Normal, Border: Top: (No border), Bottom: (No border), Left: (No border), Right: (No border), Between : (No border), Tab stops: 7.96 cm, Centred + 15.92 cm, Right

(nodes) shows the strength of the causal effect, the β value (auto β value), while the numbers on the arrows show the lag at which the causal link is detected.

To provide a fair comparison between ERA5-81 and SEAS5.1-03, we adopt the concept of causal inference (see Methods Section 2.3). Based on the results shown in Fig. 6, we now assume that the selection of causal links shown in Fig. 7a is found in both ERA5-81 and SEAS5.1-03, and also for GHGS and GHGN indices. Here, we construct the CEN network by imposing a sub-selection of all the links that PCMCi detects in Fig. 6a and 6b. Links are sub-selected to best represent the Preece23 hypothesis and to balance between links found in ERA5 and those found in SEAS5.1. Note that in Fig. 7a the maximum lag used is -1. Moreover, while in Fig. 6b the sign of the SEAS5.1 MSLP-NAm \rightarrow GGI link (lag 0) is negative, in ERA5 this link shows a positive sign (Fig. 7a). Figures 7b-e show the β values calculated for ERA5-81 and ERA5-40, together with the β value distributions obtained by bootstrapping 1000 times SEAS5.1-03 and SEAS.1-05. For links that do not include GGI (Fig. 7b), in general ERA5-81 and ERA5-40 β values fall inside the SEAS5.1-03 and SEAS.1-05 β value distributions. The AMV \rightarrow MSLP-NAm link (lag 0) show negative $\beta \sim -0.1-0.2$, with SEAS5.1 showing somewhat higher absolute values up to $\beta \sim -0.2$ (Fig. 7b). The T2m-Arctic \rightarrow Snow-NAm link (lag -1) shows the strongest causal effect with a $\beta \sim -0.3-0.5$, however, both ERA5 values are outside or at the far end of the two SEAS5.1 distributions, which are centered around $\beta \sim -0.1-0.2$. This hints to a potential underestimation of the effect of MJJ Snow on JJA MSLP over North America in SEAS5.1. In contrast, the Snow-NAm \rightarrow T2m-Arctic link (lag -1) is centered around $\beta \sim 0$ in both ERA5 and SEAS5.1, showing a negligible effect of North American snow cover on Arctic surface temperatures. Both the Snow-NAm \rightarrow MSLP-NAm link (lag -1) and the MSLP-NAm \rightarrow Snow-NAm link (lag -1) show a weak positive $\beta \sim 0.1-0.2$ on each other, with the latter being somewhat stronger in SEAS5.1.

Figures 7c, 7d and 7e show the causal links directed towards GGI, GHGS and GHGN respectively. For GGI, three links show good agreement between ERA5 and SEAS5.1, i.e. AMV \rightarrow GGI (lag 0, $\beta \sim -0.1$), T2m-Arctic \rightarrow GGI (lag 0, $\beta \sim 0.2-0.4$) and GGI \rightarrow GGI itself (lag -1, $\beta \sim 0.1-0.2$). For these links, ERA5 β values fall inside the distribution of SEAS5.1 β values. This is not the case for links T2m-Arctic \rightarrow GGI (lag -1, ERA5 $\beta \sim 0.3$, SEAS5.1 $\beta \sim 0.1$), Snow-NAm \rightarrow GGI (lag -1, ERA5 $\beta \sim -0.2$, SEAS5.1 $\beta \sim 0$) and MSLP-NAm \rightarrow GGI (lag 0, ERA5 $\beta \sim 0.1$, SEAS5.1 $\beta \sim -0.2$). For the latter, the (absolute) β values are higher in SEAS5.1 than in ERA5, while SEAS5.1 struggles to reproduce the strength of the causal effect of Snow-NAm and Arctic-T2m on GGI (Fig. 7c). GHGS (Fig. 7d) and GHGN (Fig. 7e) show similar results. However, when the two components that make GGI are analysed separately, it is possible to distinguish whether the underestimation effect in SEAS5.1 comes from the southern or norther components of the blocking gradients. E.g., the underestimation of the GGI \rightarrow Snow (lag -1) link comes from an underestimation of the GHGS \rightarrow Snow causal link

Formatted: Font: Cardo

Deleted: Figures 7b-e show the

Deleted: showing

Deleted: North America on

Deleted: 22

Formatted: Font colour: Black

Formatted: Normal, Border: Top: (No border), Bottom: (No border), Left: (No border), Right: (No border), Between : (No border), Tab stops: 7.96 cm, Centred + 15.92 cm, Right

(Fig. 7d), while the underestimation of the GGI → T2m-Arctic (lag -1) link comes from an underestimation of the GHGN → T2m-Arctic link (Fig. 7e). In general, for 7 out of the 11 causal links analyses there is a good match between ERA5 and SEAS5.1. However, SEAS5.1 seems to underestimate the links between both Arctic surface temperatures and snow cover over North America and blocking indices (Fig. 7c-e). Moreover, the influence of snow cover on MSLP over North America is also underestimated (Fig. 7b). Thus, the causal analysis supports the hypothesis that the forecast model does not correctly represent the physical effects of depleted snow cover on increased blocking over Greenland. Using the HA16 index leads to qualitatively similar results (see Fig. S16 in the Supplementary Material).

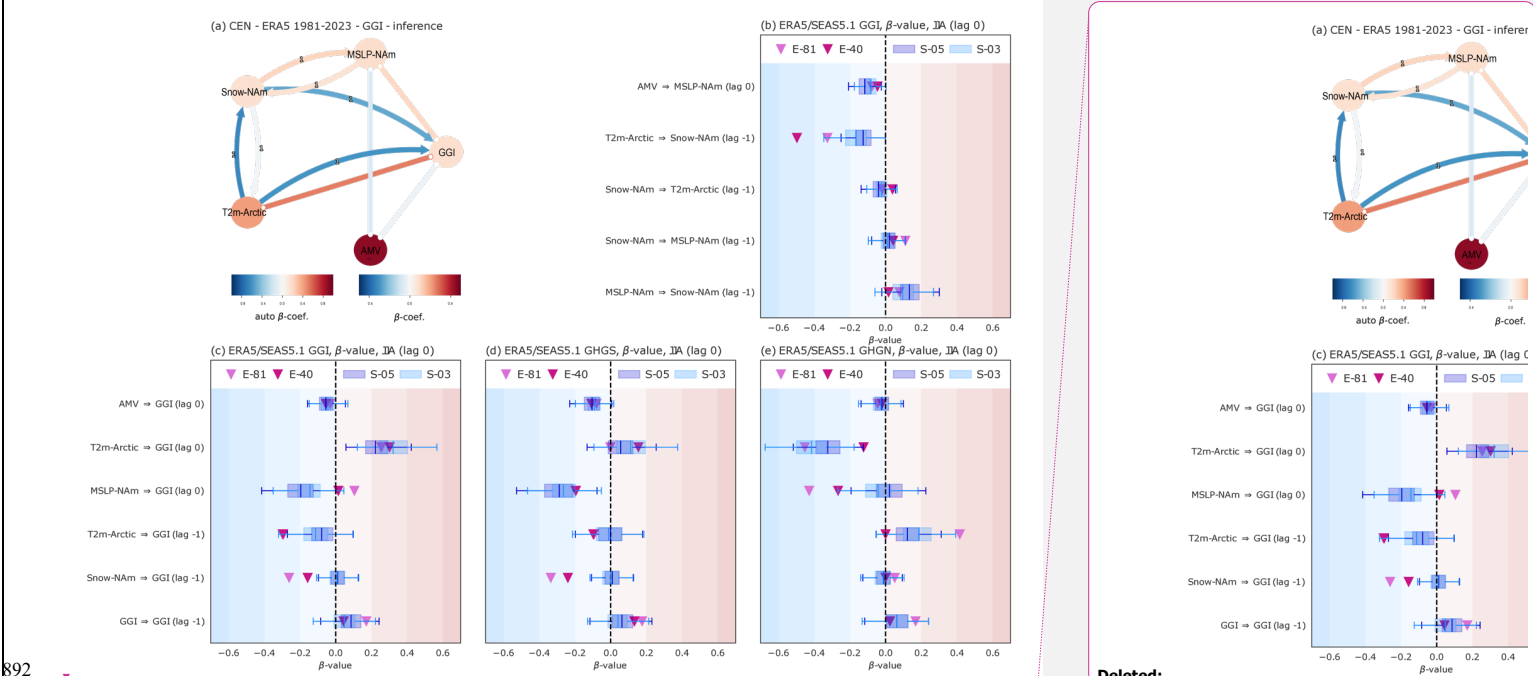


Figure 7. Causal inference for monthly potential precursors. Panel (a): inferred CEN with ERA5 MSLP-NAm, Snow-NAm, T2m-Arctic, AMV and GGI for the 1981-2023 period for both SEAS5.1-03, SEAS5.1-05, ERA5-40 and ERA5-81. Panel (b): β values for links shown in Panel (a) that do not include GGI. Panel (c): same as for Panel (b) but for links that are directed towards GGI. Panel (e) and (f): same as for Panel (c) but for GHGS and GHGN indices. The boxplots show β values calculated a 1000 time in SEAS5.1-03 and SEAS5.1-05 (whiskers show the 95% confidence interval).

Deleted:

Deleted: 23

Formatted: Font colour: Black

Formatted: Normal, Border: Top: (No border), Bottom: (No border), Left: (No border), Right: (No border), Between : (No border), Tab stops: 7.96 cm, Centred + 15.92 cm, Right

899 **4 Discussions and Conclusions**

900 In this study, we investigate whether the observed trend in summer Greenland blocking can be attributed to natural variability,

901 looking at features as the Atlantic multidecadal variability (AMV), or whether it is influenced by Arctic warming, following

902 the hypothesis proposed by Preece23. According to Preece23, Arctic warming may lead to early snow cover depletion in May,

903 which can generate a low-pressure anomaly over North America, which subsequently may act as a waveguide, resulting in

904 increased blocking over Greenland.

905 On top of this, our study aims to address a critical gap in understanding the representation of Greenland blocking within

906 advanced seasonal forecasting systems by evaluating the ECMWF SEAS5.1. Following the definition of Davini et al. (2012)

907 for the Greenland blocking index (GBI), we derived a Greenland gradient index (GGI) from its southern and northern

908 meridional components, GHGS and GHGN, to ensure a continuous time series for statistical analysis where the use of the GBI

909 was not applicable. Both blocking indices (GBI, GGI) show a positive statistically significant trend from 1940 to 2023 but

910 reveal a negative trend in the last decade. The analysis focuses on how SEAS5.1 state-of-the-art, multi-member high-resolution

911 model captures the spatial patterns, trends, and natural variability associated with Greenland blocking.

912 Using various statistical methods (linear regression, correlation analysis, causal discovery, and causal inference), we find

913 multiple evidence that both Arctic warming and natural variability have influenced Greenland blocking at monthly time scales

914 during the observational period. Our correlation and causal analyses indicate a robust relationship in ERA5, where high Arctic

915 temperatures lead to early snow cover depletion in May, which can subsequently cause a low-pressure anomaly over North

916 America (MSLP-Nam), consistent with Preece23 (Figs. 5, 6 and 7). The identified relationships are stronger over the more

917 recent time window 1981-2023 rather than the full reanalysis period 1940-2023: this is consistent with the larger impact of

918 Arctic warming in the recent years, which could have weakened the background westerly flows and this favoured stronger

919 stationary wave persistence (Hoskins and Woollings, 2015; Coomou et al, 2018).

920 While in ERA5 the direct effect of MSLP-Nam on GGI seems limited (Fig. 7c), its effect on the meridional gradient reversal

921 GHGS is consistent with Preece23: negative MSLP-Nam leads to positive GHGS anomalies (Fig. 7d). However, negative

922 MSLP-Nam also leads to positive GHGN anomalies (Fig. 7e), likely explaining the lack of signal on GGI. Snow cover

923 influences MSLP-Nam (Figs. 6a and 7b), and shows a direct effect on GGI and GHGS, but not on GHGN. Enhanced Arctic

924 temperatures also positively influence GGI and GHGS, while GHGN receives a consistent negative influence (Figs. 7c-e).

925 Overall, our analysis reveals that in ERA5, higher Arctic temperatures and reduced snow cover are associated with low-

926 pressure anomalies over North America but do not result in blocking, as defined by the index used in our study. However, we

927 observe a connection with elevated pressure highs over Greenland (GHGS > 0). This finding aligns with Preece et al. (2023),

928 where the authors apply the HA16 blocking index proposed by Hanna et al., which defines blocking as a large geopotential

929 height value over Greenland (Hanna et al., 2013). Notably, the HA16 index lacks some characteristics typically associated

930 with blocking, being mostly the presence of a westerly flow poleward of the block. The degree of similarity between this index

Deleted: Discussion

Deleted: Conclusion

Deleted: specifically

Deleted: amplification (AA),

Deleted: AA

Deleted: (

Deleted: ..

Deleted: amplification

Deleted: over the period 1981-2023

Deleted: 5b, 6a

Deleted: 7b).

Deleted: lead

Deleted: lead

Deleted: Thus

Deleted: lead to

Deleted: (2023), where the authors apply the blocking index proposed by Hanna et al., which defines blocking as positive pressure anomalies over Greenland (Hanna et al., 2013). Notably, this index lacks some characteristics typically associated with blocking.

Deleted: 24

Formatted: Font colour: Black

Formatted: Normal, Border: Top: (No border), Bottom: (No border), Left: (No border), Right: (No border), Between : (No border), Tab stops: 7.96 cm, Centred + 15.92 cm, Right

950 and GHGS > 0, as well as whether it sufficiently captures Greenland blocking, remains an open question. Addressing this gap
951 could provide valuable insights and warrants further investigation in future studies.

952

953 When focusing on SEAS5.1, it is possible to see that even with some difficulties the model is capable of reproducing the
954 observed blocking trend (only ~10% of the sub-samples show a trend that is comparable with the ERA5 trend, Fig. 2). The
955 forecast system shows consistent causal links among high Arctic temperatures, low snow cover, and low-pressure over North
956 America (Figs. 6b and 7b), which agree both with ERA5 and with the Preece23 hypothesis, although the strength of these
957 connections is generally underestimated in the model, suggesting a low signal-to-noise ratio. However, the influence of snow
958 cover on the blocking indices is the most misrepresented causal link (Figs. 7c-e). Thus, this suboptimal mechanism may explain
959 the difficulties of SEAS5.1 to replicate the historical trends in ERA5.

960 The culprit might be the misrepresentation of snow cover in SEAS5.1: May snow cover climatology in SEAS5.1 shows an
961 overestimation over western North America both in SEAS5.1-03 and SEAS.1-05 (see Supplementary Material Figs. S10o and
962 S11o respectively). This hypothesis is also supported by the strong differences in the 11-year running mean between ERA5
963 and SEAS5.1 (Fig. 4j). While SEAS5.1 data initialized in March and May shows very similar causal results (Fig. 7), using
964 SEAS5.1 initialised in June, improves at least partially the correlations among Arctic temperatures, snow cover, and low-
965 pressure over North America (Fig. S8). However, it does not improve the correlations with the blocking indices, suggesting
966 that even using snow cover values closer to the observations does not improve the representation of the snow – blocking link
967 in SEAS5.1.

968 While blocking shows multidecadal variability in its observed blocking trends, the influence of the Atlantic multidecadal
969 variability (AMV) on blocking variability is only weakly detected. The 11-year moving window trends in the blocking indices
970 (Fig. 2) and their potential drivers (Fig. 4) indicate strong variability over the observational period. The AMV shows a
971 negligible causal influence on blocking indices (Fig. 7c-e). Nevertheless, AMV has at least some influence on the pressure-
972 low and snow cover over North America (though the latter is found only on ERA5, Fig. 6), and thus has an indirect, though
973 weak, influence over blocking. The AMV shifted to a positive trend in 1981, likely enhancing the negative trend of MSLP
974 and, in turn, blocking trends. Thus, our analysis shows that the combination of high Arctic warming and a positive AMV phase
975 likely favour enhanced blocking over Greenland. However, in the past six years, we observed a weakening in the blocking
976 trend (Fig. 2), despite a steady increase in Arctic temperature and decrease in low-pressure over North America (Figs. 4j and
977 4k respectively), indicating that internal variability might be overshadowing the Arctic warming signal. In fact, in that same
978 period a small positive trend in the Snow cover of North America was observed, which could explain the dampening of the
979 blocking. If this mechanism holds, we could further speculate in the short-term that the positive phases of the AMV will
980 enhance the probability of low pressure over North America, thereby increasing both GHGS and GHGN. However, if snow
981 cover will continue to decrease, positive values of GHGS may prevail, favouring larger blocking frequencies.

982

Formatted: Not Highlight

Deleted: While SEAS5.1 struggles to reproduce

Deleted: 2), our analysis sheds light on the ability of the forecasting model in reproducing the physical mechanisms observed in ERA5. SEAS5.1

Deleted: missed

Deleted: help explaining

Deleted: A potential explanation for this missed link may

Deleted: that

Deleted: itself is misrepresented

Deleted:

Deleted: (

Deleted:).

Deleted: misrepresentation

Deleted: running mean

Deleted: AA

Deleted: 25

Formatted: Font colour: Black

Formatted: Normal, Border: Top: (No border), Bottom: (No border), Left: (No border), Right: (No border), Between : (No border), Tab stops: 7.96 cm, Centred + 15.92 cm, Right

998 Blocking is important for Greenland surface temperatures and Greenland melting events (Hanna et al., 2018; McLeod and
999 Mote, 2016; Sasgen et al., 2020). Thus, the uncertainty in how climate models can reproduce blocking variability and trends
1000 (Delhasse et al., 2020; Maddison et al., 2024) represents a challenge to correctly estimate the future changes that will affect
1001 the Greenland ice sheet. Our analysis builds confidence that the ECMWF seasonal forecasting system can reproduce, though
1002 rarely, the observed trend, highlighting the limitation of CMIP6 where none of the models is able to replicate the trend.
1003 Moreover, the seasonal forecast model can represent most of the Arctic – blocking links, apart from the direct link of snow
1004 cover on blocking. Thus, while blocking over Greenland does not show increasing trends in future projections (Davini and
1005 D’Andrea, 2020), we show that there is a reasonable chance that the lack of this trend is explained by suboptimal representation
1006 of the snow – blocking mechanisms in the model.

1007 Future changes in the causal drivers of blocking can then provide us with an estimation of the potential effect that these changes
1008 may have on blocking itself. Snow cover extent over North America will keep declining (O’Gorman, 2014; Quante et al.,
1009 2021) while Arctic temperatures are projected to keep increasing under anthropogenic climate change (Cai et al., 2021; Hu et
1010 al., 2021; Shu et al., 2022). This combined effect has the potential to contribute to increased blocking over Greenland and then
1011 accelerate melting of its ice sheet. However, the amount of snowfall in winter is probably influenced by large-scale oceanic
1012 and atmospheric patterns (Lundquist et al., 2023) meaning that climate variability will continue to influence blocking. Thus,
1013 while blocking will still be modulated by the AMV or other sources of natural variability, in the long term, snow cover will
1014 decline due to the dominant forces of climate change, potentially leading to increased blocking. Of course, changes in tropical
1015 regions, or changes in these teleconnection pathways (Meehl et al., 2018a, Zhu et al., 2024) can potentially enhance the effect
1016 of climate change in Arctic regions however, it is worth mentioning that we explored the potential linkage between El Niño
1017 Southern Oscillation (ENSO) making use of the PCMCI methodology and no evident linkage emerges between the NINO3.4
1018 index and any of the Greenland blocking used.

1019 ▼

1020 To summarize, we investigated the role of snow cover over North America, Arctic amplification and Atlantic multidecadal
1021 variability in influencing Greenland blocking trends. Our findings suggest that higher Arctic temperatures lead to early snow
1022 cover depletion, causing low-pressure anomalies over North America, which may increase blocking over Greenland, in
1023 alignment with the theory proposed by Preece et al (2023).

1024 On top of this, this work looks at different components of Greenland blocking, thus identifying the specific effect of each
1025 causal driver on both its southern and northern meridional components. The ECMWF SEAS5.1 model struggles to accurately
1026 represent the causal links between Arctic temperatures, snow cover, and surface pressure patterns, potentially limiting its
1027 ability to reproduce observed blocking trends. Indeed, SEAS5.1 can reproduce the Arctic temperature – snow cover – low
1028 pressure links while struggling in reproducing the direct causal link between snow cover and Greenland blocking, hinting at a
1029 potential missing physical mechanism that may explain the discrepancy between observed and modelled trends. ▼

1030 However, a negative blocking trend in the last decade challenges the idea that Arctic warming is the main driver of changes in
1031 atmospheric blocking over Greenland. Thus, the recent decline in the observed blocking trend, despite stable Arctic

Deleted: , and as a consequence, the impact of the latter on sea level rise (Beckmann and Winkelmann, 2023).

Deleted: with the exception of

Deleted: at least

Deleted: While our analysis shows that positive phases of the AMV can enhance blocking activity over Greenland, the AMV variability is projected to decrease in future projections from CMIP6 models (Shang et al., 2024). Moreover, AMV variability is also too weak in CMIP5 and CMIP6 models (Bracegirdle, 2022), thus potentially affecting its effect on blocking.

Deleted: Nonetheless, long-term future Arctic temperatures could shift snowfall to rainfall (Collins et al., 2024; McCrystall et al., 2021).

Commented [8]: @giorgia.dicapua@gmail.com could it make sense a sentence like this?

Deleted: While future projections show a steady decline of mean snow cover over northern latitudes (O’Gorman, 2015; Diro and Sushama, 2020; Mudryk et al., 2020; Quante et al., 2021) observations show an increase in snow cover over the past decade (Cohen et al., 2020). This trend may be explained by changes in several mid-latitude and polar drivers, such as meandering of tropospheric circulation (Di Capua and Coumou, 2016; Francis and Vavrus, 2015), Arctic Amplification (Cohen et al., 2020) and polar vortex variability (Cellitti et al., 2006; Kretschmer et al., 2018a,b ; Overland and Wang, 2019). On the other hand, tropical – extratropical (Arctic) teleconnection can affect the circulation patterns and climate variability in the Arctic regions (Meehl et al., 2018a; Ye and Jung, 2019). Convective activity variability of both tropical Pacific and Atlantic Oceans are partially responsible for negative trends in Arctic sea ice extent in the past decades (Meehl et al., 2018a) and tropical Indo-Pacific convection can induce a poleward-propagating Rossby wave train, which in turn affects surface temperature over the Arctic Archipelago during summer (Zhu et al., 2024). Thus, changes in tropical regions, or changes in these teleconnection pathways, can potentially enhance the effect of climate change in Arctic regions. ▲

Deleted: , in this study

Deleted: Moreover

Deleted: to

Deleted: The model misrepresentation of other phenomena at play, like the AMV variability, which shows at least some indirect influence on blocking, and tropical drivers, which are not directly considered in this study, may also provide further source for uncertainty. Furthermore

Deleted: amplification

Deleted: 26

Formatted: Font colour: Black

Formatted: Normal, Border: Top: (No border), Bottom: (No border), Left: (No border), Right: (No border), Between : (No border), Tab stops: 7.96 cm, Centred + 15.92 cm, Right

temperature increases, indicates that other factors may be at play. Despite the above-mentioned limitations, SEAS5.1 can reproduce the observed Greenland blocking trend in only 10% of its samples but does not rule entirely the possibility that natural variability is playing a considerable role in the current observed trend of summer Greenland blocking. This of course opens the question to what extent such linkage might be affecting other regions in the high latitudes and offsetting other long-term predictions in global climate models. Future work is needed to further assess the capability of historical and future projections provided by CMIP6 models in representing this snow – blocking mechanisms, to evaluate the reliability of future trends in blocking over Greenland.

Data availability. The data used in this article can be accessed by contacting the corresponding author. ERA5 (<https://doi.org/10.24381/cds.50ed0a73>, Copernicus Climate Change Service, Climate Data Store, 2018) and SEAS5.1 (<https://doi.org/10.24381/cds.adbb2d47>, Hersbach et al., 2023) datasets are publicly available on the Copernicus website.

Supplement. The supplement related to this article is available.

Author contributions. J.B., G.D.C. and P.D. equally contributed to the design of the analysis. J.B. and G.D.C. performed the analysis and wrote the first draft of the paper. J.B., G.D.C. and P.D. contributed to the interpretation of the results and to the writing of the paper.

Competing interests. The contact author has declared that none of the authors has any competing interests.

Acknowledgements. We thank Efi Rousi for the valuable discussions at the onset of this research project.

Financial support. This research has been supported by the German Federal Ministry for Education and Research (BMBF) via the JPI Climate/JPI Oceans project ROADMAP (grant no. 01LP2002B) (G.D.C.) and via the ClimXtreme project (subproject PERSEVERE, phase 2nd, grant no. 01LP2322D) (G.D.C.). J.B. was further supported by the Australian Research Council Special Research Initiative Securing Antarctica’s Environmental Future (SR200100005).

References

- Baxter, I., Ding, Q., Schweiger, A., L’Heureux, M., Baxter, S., Wang, T., Zhang, Q., Harnos, K., Markle, B., Topal, D., and Lu, J.: How Tropical Pacific Surface Cooling Contributed to Accelerated Sea Ice Melt from 2007 to 2012 as Ice Is Thinned by Anthropogenic Forcing, *Journal of Climate*, 32, 8583–8602, <https://doi.org/10.1175/JCLI-D-18-0783.1>, 2019.
- Beckmann, J. and Winkelmann, R.: Effects of extreme melt events on ice flow and sea level rise of the Greenland Ice Sheet, *The Cryosphere*, 17, 3083–3099, <https://doi.org/10.5194/tc-17-3083-2023>, 2023.

Deleted: ,

Commented [9]: a crazy idea for our future selves:: such 10% of samples which show a trend, do they have a better representation of the snow/blocking linkage?

Commented [10R9]: didn’t we check?

Commented [11R9]: gosh, I do not remember! could be...

Formatted: Font: Times New Roman, Pattern: Clear, Highlight

Deleted: Baxter, I., Ding, Q., Schweiger, A., L’Heureux, M., Baxter, S., Wang, T., Zhang, Q., Harnos, K., Markle, B., Topal, D., and Lu, J.: How Tropical Pacific Surface Cooling Contributed to Accelerated Sea Ice Melt from 2007 to 2012 as Ice Is Thinned by Anthropogenic Forcing, *Journal of Climate*, 32, 8583–8602, <https://doi.org/10.1175/JCLI-D-18-0783.1>, 2019.

Beckmann, J. and Winkelmann, R.: Effects of extreme melt events on ice flow and sea level rise of the Greenland Ice Sheet, *The Cryosphere*, 17, 3083–3099, <https://doi.org/10.5194/tc-17-3083-2023>, 2023.

Benjamini, Y. and Hochberg, Y.: Controlling the False Discovery Rate: a Practical and Powerful Approach to Multiple Testing, *Journal of the Royal Statistical Society. Series B (Methodological)*, 57, 289–300, <https://doi.org/10.2307/2346101>, 1995.

Blackport, R. and Screen, J. A.: Insignificant effect of Arctic amplification on the amplitude of midlatitude atmospheric waves, *Sci. Adv.*, 6, eay2880, <https://doi.org/10.1126/sciadv.aay2880>, 2020.

Blau, M. T., Ha, K.-J., and Chung, E.-S.: Extreme summer temperature anomalies over Greenland largely result from clear-sky radiation and circulation anomalies, *Commun Earth Environ*, 5, 405, <https://doi.org/10.1038/s43247-024-01549-7>, 2024.

Bracegirdle, T. J.: Early-to-Late Winter 20th Century North Atlantic Multidecadal Atmospheric Variability in Observations, CMIP5 and CMIP6, *Geophysical Research Letters*, 49, e2022GL098212, <https://doi.org/10.1029/2022GL098212>, 2022.

Cai, W., Santoso, A., Wang, G., Yeh, S.-W., An, S.-I., Cobb, K. M., Collins, M., Guilyardi, E., Jin, F.-F., Kug, J.-S., Lengaigne, M., McPhaden, M. J., Takahashi, K., Timmermann, A., Vecchi, G., Watanabe, M., and Wu, L.: ENSO and greenhouse warming, *Nature Clim Change*, 5, 849–859, <https://doi.org/10.1038/nclimate2743>, 2015.

Cai, Z., You, Q., Wu, F., Chen, H. W., Chen, D., and Cohen, J.: Arctic Warming Revealed by Multiple CMIP6 Models: Evaluation of Historical Simulations and Quantification of Future Projection Uncertainties, *Journal of Climate*, 34, 4871–4892, <https://doi.org/10.1175/JCLI-D-20-0791.1>, 2021.

Di Capua, G., Sparrow, S., Kornhuber, K., Rousi, E., Osprey, S., Wallom, D., van den Hurk, B., and Coumou, D.: Drivers behind the summer 2010 wave train leading to Russian heatwave and Pakistan flooding, *npj Climate and Atmospheric Science*, 4, <https://doi.org/10.1038/s41612-021-00211-9>, 2021.

Cellitti, M. P., Walsh, J. E., Rauber, R. M., and Portis, D. H.: Extreme cold air outbreaks over the United States, the polar vortex, and the large-scale circulation, *J. Geophys. Res.*, 111, 2005JD006273, <https://doi.org/10.1029/2005JD006273>, 2006. ... [9]

Deleted: 27

Formatted: Font colour: Black

Formatted: Normal, Border: Top: (No border), Bottom: (No border), Left: (No border), Right: (No border), Between : (No border), Tab stops: 7.96 cm, Centred + 15.92 cm, Right

Benjamini, Y. and Hochberg, Y.: Controlling the False Discovery Rate: a Practical and Powerful Approach to Multiple Testing, *Journal of the Royal Statistical Society. Series B (Methodological)*, 57, 289–300, <https://doi.org/10.2307/2346101>, 1995.

Blackport, R. and Screen, J. A.: Insignificant effect of Arctic amplification on the amplitude of midlatitude atmospheric waves, *Sci. Adv.*, 6, eaay2880, <https://doi.org/10.1126/sciadv.aay2880>, 2020.

Blau, M. T., Ha, K.-J., and Chung, E.-S.: Extreme summer temperature anomalies over Greenland largely result from clear-sky radiation and circulation anomalies, *Commun Earth Environ*, 5, 405, <https://doi.org/10.1038/s43247-024-01549-7>, 2024.

Bracegirdle, T. J.: Early-to-Late Winter 20th Century North Atlantic Multidecadal Atmospheric Variability in Observations, CMIP5 and CMIP6, *Geophysical Research Letters*, 49, e2022GL098212, <https://doi.org/10.1029/2022GL098212>, 2022.

Cai, W., Santoso, A., Wang, G., Yeh, S.-W., An, S.-I., Cobb, K. M., Collins, M., Guilyardi, E., Jin, F.-F., Kug, J.-S., Lengaigne, M., McPhaden, M. J., Takahashi, K., Timmermann, A., Vecchi, G., Watanabe, M., and Wu, L.: ENSO and greenhouse warming, *Nature Clim Change*, 5, 849–859, <https://doi.org/10.1038/nclimate2743>, 2015.

Cai, Z., You, Q., Wu, F., Chen, H. W., Chen, D., and Cohen, J.: Arctic Warming Revealed by Multiple CMIP6 Models: Evaluation of Historical Simulations and Quantification of Future Projection Uncertainties, *Journal of Climate*, 34, 4871–4892, <https://doi.org/10.1175/JCLI-D-20-0791.1>, 2021.

Di Capua, G., Sparrow, S., Kornhuber, K., Rousi, E., Osprey, S., Wallom, D., van den Hurk, B., and Coumou, D.: Drivers behind the summer 2010 wave train leading to Russian heatwave and Pakistan flooding, *npj Climate and Atmospheric Science*, 4, <https://doi.org/10.1038/s41612-021-00211-9>, 2021.

Cellitti, M. P., Walsh, J. E., Rauber, R. M., and Portis, D. H.: Extreme cold air outbreaks over the United States, the polar vortex, and the large-scale circulation, *J. Geophys. Res.*, 111, 2005JD006273, <https://doi.org/10.1029/2005JD006273>, 2006.

Chen, L., Li, T., Yu, Y., and Behera, S. K.: A possible explanation for the divergent projection of ENSO amplitude change under global warming, *Clim Dyn*, 49, 3799–3811, <https://doi.org/10.1007/s00382-017-3544-x>, 2017.

Cohen, J., Screen, J. A., Furtado, J. C., Barlow, M., Whittleston, D., Coumou, D., Francis, J., Dethloff, K., Entekhabi, D., Overland, J., and Jones, J.: Recent Arctic amplification and extreme mid-latitude weather, *Nature Geosci*, 7, 627–637, <https://doi.org/10.1038/ngeo2234>, 2014.

Cohen, J., Zhang, X., Francis, J., Jung, T., Kwok, R., Overland, J., Ballinger, T. J., Bhatt, U. S., Chen, H. W., Coumou, D., Feldstein, S., Gu, H., Handorf, D., Henderson, G., Ionita, M., Kretschmer, M., Laliberte, F., Lee, S., Linderholm, H. W., Maslowski, W., Peings, Y., Pfeiffer, K., Rigor, I., Semmler, T., Stroeve, J., Taylor, P. C., Vavrus, S., Vihma, T., Wang, S., Wendisch, M., Wu, Y., and Yoon, J.: Divergent consensus on Arctic amplification influence on midlatitude severe winter weather, *Nat. Clim. Chang.*, 10, 20–29, <https://doi.org/10.1038/s41558-019-0662-y>, 2020.

Collins, M., Beverley, J. D., Bracegirdle, T. J., Catto, J., McCrystall, M., Dittus, A., Freychet, N., Grist, J., Hegerl, G. C., Holland, P. R., Holmes, C., Josey, S. A., Joshi, M., Hawkins, E., Lo, E., Lord, N., Mitchell, D., Monerie, P.-A., Priestley, M. D. K., Scaife, A., Screen, J., Senior, N., Sexton, D., Shuckburgh, E., Siegert, S., Simpson, C., Stephenson, D. B., Sutton, R., Thompson, V., Wilcox, L. J., and Woollings, T.: Emerging signals of climate change from the equator to the poles: new insights into a warming world, *Front. Sci.*, 2, 1340323, <https://doi.org/10.3389/fsci.2024.1340323>, 2024.

Coumou, D., Di Capua, G., Vavrus, S., Wang, L., and Wang, S.: The influence of Arctic amplification on mid-latitude summer circulation, *Nat Commun*, 9, 2959, <https://doi.org/10.1038/s41467-018-05256-8>, 2018.

Deleted: 28*

Formatted: Font colour: Black

Formatted: Normal, Border: Top: (No border), Bottom: (No border), Left: (No border), Right: (No border), Between : (No border), Tab stops: 7.96 cm, Centred + 15.92 cm, Right

1262 Davini, P. and D'Andrea, F.: Northern Hemisphere Atmospheric Blocking Representation in Global Climate Models: Twenty
1263 Years of Improvements?, Journal of Climate, 29, 8823–8840, <https://doi.org/10.1175/JCLI-D-16-0242.1>, 2016.

1264 Davini, P. and D'Andrea, F.: From CMIP3 to CMIP6: Northern Hemisphere Atmospheric Blocking Simulation in Present and
1265 Future Climate, Journal of Climate, 33, 10021–10038, <https://doi.org/10.1175/JCLI-D-19-0862.1>, 2020.

1266 Davini, P., Cagnazzo, C., Gualdi, S., and Navarra, A.: Bidimensional Diagnostics, Variability, and Trends of Northern
1267 Hemisphere Blocking, Journal of Climate, 25, 6496–6509, <https://doi.org/10.1175/JCLI-D-12-00032.1>, 2012.

1268 Davini, P., Weisheimer, A., Balmaseda, M., Johnson, S. J., Molteni, F., Roberts, C. D., Senan, R., and Stockdale, T. N.: The
1269 representation of winter Northern Hemisphere atmospheric blocking in ECMWF seasonal prediction systems, Quart J Royal
1270 Meteor Soc, 147, 1344–1363, <https://doi.org/10.1002/qj.3974>, 2021.

1271 Davy, R., Chen, L., and Hanna, E.: Arctic amplification metrics, Intl Journal of Climatology, 38, 4384–4394,
1272 <https://doi.org/10.1002/joc.5675>, 2018.

1273 Delhasse, A., Hanna, E., Kittel, C., and Fettweis, X.: Brief communication: CMIP6 does not suggest any circulation change
1274 over Greenland in summer by 2100, Ice sheets/Atmospheric Interactions, <https://doi.org/10.5194/tc-2019-332>, 2020.

1275 Di Capua, G. and Coumou, D.: Changes in meandering of the Northern Hemisphere circulation, Environ. Res. Lett., 11,
1276 094028, <https://doi.org/10.1088/1748-9326/11/9/094028>, 2016.

1277 Di Capua, G., Kretschmer, M., Runge, J., Alessandri, A., Donner, R. V., Van Den Hurk, B., Vellore, R., Krishnan, R., and
1278 Coumou, D.: Long-Lead Statistical Forecasts of the Indian Summer Monsoon Rainfall Based on Causal Precursors, Weather
1279 and Forecasting, 34, 1377–1394, <https://doi.org/10.1175/WAF-D-19-0002.1>, 2019.

1280 Di Capua, G., Runge, J., Donner, R. V., Van Den Hurk, B., Turner, A. G., Vellore, R., Krishnan, R., and Coumou, D.: Dominant
1281 patterns of interaction between the tropics and mid-latitudes in boreal summer: causal relationships and the role of timescales,
1282 Weather Clim. Dynam., 1, 519–539, <https://doi.org/10.5194/wcd-1-519-2020>, 2020a.

1283 Di Capua, G., Kretschmer, M., Donner, R. V., Van Den Hurk, B., Vellore, R., Krishnan, R., and Coumou, D.: Tropical and
1284 mid-latitude teleconnections interacting with the Indian summer monsoon rainfall: a theory-guided causal effect network
1285 approach, Earth Syst. Dynam., 11, 17–34, <https://doi.org/10.5194/esd-11-17-2020>, 2020b.

1286 Di Capua, G., Coumou, D., Van Den Hurk, B., Weisheimer, A., Turner, A. G., and Donner, R. V.: Validation of boreal summer
1287 tropical–extratropical causal links in seasonal forecasts, Weather Clim. Dynam., 4, 701–723, <https://doi.org/10.5194/wcd-4-701-2023>, 2023.

1288

1289 Di Capua, G., Tyrllis, E., Matei, D., and Donner, R. V.: Tropical and mid-latitude causal drivers of the eastern Mediterranean
1290 Etesians during boreal summer, Clim Dyn, 62, 9565–9585, <https://doi.org/10.1007/s00382-024-07411-y>, 2024.

1291 Ding, Q., Wallace, J. M., Battisti, D. S., Steig, E. J., Gallant, A. J. E., Kim, H.-J., and Geng, L.: Tropical forcing of the recent
1292 rapid Arctic warming in northeastern Canada and Greenland, Nature, 509, 209–212, <https://doi.org/10.1038/nature13260>,
1293 2014.

1294 Diro, G. T. and Sushama, L.: Contribution of Snow Cover Decline to Projected Warming Over North America, Geophysical
1295 Research Letters, 47, e2019GL084414, <https://doi.org/10.1029/2019GL084414>, 2020.

1296 Docquier, D., Di Capua, G., Donner, R. V., Pires, C. A. L., Simon, A., and Vannitsem, S.: A comparison of two causal methods
1297 in the context of climate analyses, Nonlin. Processes Geophys., 31, 115–136, <https://doi.org/10.5194/npg-31-115-2024>, 2024.

Deleted: 29

Formatted: Font colour: Black

Formatted: Normal, Border: Top: (No border), Bottom: (No border), Left: (No border), Right: (No border), Between : (No border), Tab stops: 7.96 cm, Centred + 15.92 cm, Right

1298 [Feldstein, S. B.: The Timescale, Power Spectra, and Climate Noise Properties of Teleconnection Patterns, *J. Climate*, 13,](#)
1299 [4430–4440, \[https://doi.org/10.1175/1520-0442\\(2000\\)013<4430:TTPSAC>2.0.CO;2\]\(https://doi.org/10.1175/1520-0442\(2000\)013<4430:TTPSAC>2.0.CO;2\), 2000.](#)

1300 [Francis, J. and Skific, N.: Evidence linking rapid Arctic warming to mid-latitude weather patterns, *Phil. Trans. R. Soc. A.*, 373,](#)
1301 [20140170, <https://doi.org/10.1098/rsta.2014.0170>, 2015.](#)

1302 [Francis, J. A. and Vavrus, S. J.: Evidence for a wavier jet stream in response to rapid Arctic warming, *Environ. Res. Lett.*, 10,](#)
1303 [014005, <https://doi.org/10.1088/1748-9326/10/1/014005>, 2015.](#)

1304 [Gan, R., Huang, G., and Hu, K.: The Diverse Impacts of El Niño on Northeastern Canada and Greenland Surface Air](#)
1305 [Temperatures, *Journal of Climate*, 37, 335–348, <https://doi.org/10.1175/JCLI-D-22-0677.1>, 2024.](#)

1306 [Gollan, G., Greatbatch, R. J., and Jung, T.: Origin of variability in Northern Hemisphere winter blocking on interannual to](#)
1307 [decadal timescales, *Geophysical Research Letters*, 42, <https://doi.org/10.1002/2015GL066572>, 2015.](#)

1308 [Häkkinen, S., Rhines, P. B., and Worthen, D. L.: Atmospheric Blocking and Atlantic Multidecadal Ocean Variability, *Science*,](#)
1309 [334, 655–659, <https://doi.org/10.1126/science.1205683>, 2011.](#)

1310 [Hanna, E., Cropper, T.E., Hall, R.J. and Cappelen, J. \(2016\). Greenland Blocking Index 1851–2015: a regional climate change](#)
1311 [signal. *Int. J. Climatol.*, 36: 4847–4861. <https://doi.org/10.1002/joc.4673>](#)

1312 [Hanna, E., Jones, J. M., Cappelen, J., Mernild, S. H., Wood, L., Steffen, K., and Huybrechts, P.: The influence of North Atlantic](#)
1313 [atmospheric and oceanic forcing effects on 1900–2010 Greenland summer climate and ice melt/runoff, *Intl Journal of*](#)
1314 [Climatology](#), 33, 862–880, <https://doi.org/10.1002/joc.3475>, 2013.

1315 [Hanna, E., Fettweis, X., Mernild, S. H., Cappelen, J., Ribergaard, M. H., Shuman, C. A., Steffen, K., Wood, L., and Mote, T.](#)
1316 [L.: Atmospheric and oceanic climate forcing of the exceptional Greenland ice sheet surface melt in summer 2012, *Intl Journal*](#)
1317 [of Climatology](#), 34, 1022–1037, <https://doi.org/10.1002/joc.3743>, 2014.

1318 [Hanna, E., Fettweis, X., and Hall, R. J.: Brief communication: Recent changes in summer Greenland blocking captured by](#)
1319 [none of the CMIP5 models, *The Cryosphere*, 12, 3287–3292, <https://doi.org/10.5194/tc-12-3287-2018>, 2018.](#)

1320 [Hauser, S., Teubler, F., Riemer, M., Knippertz, P., and Grams, C. M.: Life cycle dynamics of Greenland blocking from a](#)
1321 [potential vorticity perspective, *Weather Clim. Dynam.*, 5, 633–658, <https://doi.org/10.5194/wcd-5-633-2024>, 2024.](#)

1322 [Hersbach, H., Bell, B., Berrisford, P., Hirahara, S., Horányi, A., Muñoz-Sabater, J., Nicolas, J., Peubey, C., Radu, R., Schepers,](#)
1323 [D., Simmons, A., Soci, C., Abdalla, S., Abellan, X., Balsamo, G., Bechtold, P., Biavati, G., Bidlot, J., Bonavita, M., De Chiara,](#)
1324 [G., Dahlgren, P., Dee, D., Diamantakis, M., Dragani, R., Flemming, J., Forbes, R., Fuentes, M., Geer, A., Haimberger, L.,](#)
1325 [Healy, S., Hogan, R. J., Hólm, E., Janisková, M., Keeley, S., Laloyaux, P., Lopez, P., Lupu, C., Radnoti, G., De Rosnay, P.,](#)
1326 [Rozum, I., Vamborg, F., Villaume, S., and Thépaut, J.: The ERA5 global reanalysis, *Quart J Royal Meteor Soc*, 146, 1999–](#)
1327 [2049, <https://doi.org/10.1002/qj.3803>, 2020.](#)

1328 [Hoskins, B., & Woollings, T. \(2015\). Persistent Extratropical Regimes and Climate Extremes. *Current Climate Change*](#)
1329 [Reports](#), 1(3), 115–124. <https://doi.org/10.1007/s40641-015-0020-8>

1330 [Hu, C., Yang, S., Wu, Q., Li, Z., Chen, J., Deng, K., Zhang, T., and Zhang, C.: Shifting El Niño inhibits summer Arctic](#)
1331 [warming and Arctic sea-ice melting over the Canada Basin, *Nat Commun*, 7, 11721, <https://doi.org/10.1038/ncomms11721>,](#)
1332 [2016.](#)

Deleted: 30*

Formatted: Font colour: Black

Formatted: Normal, Border: Top: (No border), Bottom: (No border), Left: (No border), Right: (No border), Between : (No border), Tab stops: 7.96 cm, Centred + 15.92 cm, Right

1B33 [Hu, X.-M., Ma, J.-R., Ying, J., Cai, M., and Kong, Y.-Q.: Inferring future warming in the Arctic from the observed global](#)
1B34 [warming trend and CMIP6 simulations, *Advances in Climate Change Research*, 12, 499–507,](#)
1B35 <https://doi.org/10.1016/j.accre.2021.04.002>, 2021.

1B36 [Johnson, S. J., Stockdale, T. N., Ferranti, L., Balmaseda, M. A., Molteni, F., Magnusson, L., Tietsche, S., Decremer, D.,](#)
1B37 [Weisheimer, A., Balsamo, G., Keeley, S. P. E., Mogensen, K., Zuo, H., and Monge-Sanz, B. M.: SEAS5: the new ECMWF](#)
1B38 [seasonal forecast system, *Geosci. Model Dev.*, 12, 1087–1117, https://doi.org/10.5194/gmd-12-1087-2019](#), 2019.

1B39 [Kohyama, T., Hartmann, D. L., and Battisti, D. S.: La Niña-like Mean-State Response to Global Warming and Potential](#)
1B40 [Oceanic Roles, *Journal of Climate*, 30, 4207–4225, https://doi.org/10.1175/JCLI-D-16-0441.1](#), 2017.

1B41 [Kretschmer, M., Coumou, D., Donges, J. F., and Runge, J.: Using Causal Effect Networks to Analyze Different Arctic Drivers](#)
1B42 [of Midlatitude Winter Circulation, *Journal of Climate*, 29, 4069–4081, https://doi.org/10.1175/JCLI-D-15-0654.1](#), 2016.

1B43 [Kretschmer, M., Coumou, D., Agel, L., Barlow, M., Tziperman, E., and Cohen, J.: More-Persistent Weak Stratospheric Polar](#)
1B44 [Vortex States Linked to Cold Extremes, *Bulletin of the American Meteorological Society*, 99, 49–60,](#)
1B45 <https://doi.org/10.1175/BAMS-D-16-0259.1>, 2018a.

1B46 [Kretschmer, M., Cohen, J., Matthias, V., Runge, J., and Coumou, D.: The different stratospheric influence on cold-extremes](#)
1B47 [in Eurasia and North America, *npj Clim Atmos Sci*, 1, 44, https://doi.org/10.1038/s41612-018-0054-4](#), 2018b.

1B48 [Lehmann, J., Kretschmer, M., Schauburger, B., and Wechsung, F.: Potential for Early Forecast of Moroccan Wheat Yields](#)
1B49 [Based on Climatic Drivers, *Geophysical Research Letters*, 47, e2020GL087516, https://doi.org/10.1029/2020GL087516](#),
1B50 [2020.](#)

1B51 [Liu, J., Chen, Z., Francis, J., Song, M., Mote, T., and Hu, Y.: Has Arctic Sea Ice Loss Contributed to Increased Surface Melting](#)
1B52 [of the Greenland Ice Sheet?, *Journal of Climate*, 29, 3373–3386, https://doi.org/10.1175/JCLI-D-15-0391.1](#), 2016.

1B53 [Lundquist, J. D., Kim, R. S., Durand, M., and Prugh, L. R.: Seasonal Peak Snow Predictability Derived From Early-Season](#)
1B54 [Snow in North America, *Geophysical Research Letters*, 50, e2023GL103802, https://doi.org/10.1029/2023GL103802](#), 2023.

1B55 [Luu, L. N., Hanna, E., De Alwis Pitts, D., Maddison, J., Screen, J. A., Catto, J. L., and Fettweis, X.: Greenland summer](#)
1B56 [blocking characteristics: an evaluation of a high-resolution multi-model ensemble, *Clim Dyn*, 62, 10503–10523,](#)
1B57 <https://doi.org/10.1007/s00382-024-07453-2>, 2024.

1B58 [Maddison, J. W., Catto, J. L., Hanna, E., Luu, L. N., and Screen, J. A.: Missing Increase in Summer Greenland Blocking in](#)
1B59 [Climate Models, *Geophysical Research Letters*, 51, e2024GL108505, https://doi.org/10.1029/2024GL108505](#), 2024.

1B60 [Masato, G., Hoskins, B. J., and Woollings, T.: Winter and Summer Northern Hemisphere Blocking in CMIP5 Models, *Journal*](#)
1B61 [of Climate, 26, 7044–7059, https://doi.org/10.1175/JCLI-D-12-00466.1, 2013.](#)

1B62 [Matsumura, S. and Kosaka, Y.: Arctic–Eurasian climate linkage induced by tropical ocean variability, *Nat Commun*, 10, 3441,](#)
1B63 <https://doi.org/10.1038/s41467-019-11359-7>, 2019.

1B64 [Matsumura, S., Yamazaki, K., and Suzuki, K.: Slow-down in summer warming over Greenland in the past decade linked to](#)
1B65 [central Pacific El Niño, *Commun Earth Environ*, 2, 257, https://doi.org/10.1038/s43247-021-00329-x](#), 2021.

1B66 [McCrystall, M. R., Stroeve, J., Serreze, M., Forbes, B. C., and Screen, J. A.: New climate models reveal faster and larger](#)
1B67 [increases in Arctic precipitation than previously projected, *Nat Commun*, 12, 6765, https://doi.org/10.1038/s41467-021-](#)
1B68 [27031-y](#), 2021.

Deleted: 31

Formatted: Font colour: Black

Formatted: Normal, Border: Top: (No border), Bottom: (No border), Left: (No border), Right: (No border), Between : (No border), Tab stops: 7.96 cm, Centred + 15.92 cm, Right

McGraw, M. C. and Barnes, E. A.: New Insights on Subseasonal Arctic–Midlatitude Causal Connections from a Regularized Regression Model, *Journal of Climate*, 33, 213–228, <https://doi.org/10.1175/JCLI-D-19-0142.1>, 2020.

McLeod, J. T. and Mote, T. L.: Linking interannual variability in extreme Greenland blocking episodes to the recent increase in summer melting across the Greenland ice sheet: EXTREME GREENLAND BLOCKING AND SUMMER MELTING ACROSS THE GREENLAND ICE SHEET, *Int. J. Climatol.*, 36, 1484–1499, <https://doi.org/10.1002/joc.4440>, 2016.

Meehl, G. A., Chung, C. T. Y., Arblaster, J. M., Holland, M. M., and Bitz, C. M.: Tropical Decadal Variability and the Rate of Arctic Sea Ice Decrease, *Geophysical Research Letters*, 45, <https://doi.org/10.1029/2018GL079989>, 2018.

Mudryk, L., Santolaria-Otín, M., Krinner, G., Ménégot, M., Derksen, C., Brutel-Vuilmet, C., Brady, M., and Essery, R.: Historical Northern Hemisphere snow cover trends and projected changes in the CMIP6 multi-model ensemble, *The Cryosphere*, 14, 2495–2514, <https://doi.org/10.5194/tc-14-2495-2020>, 2020.

Nakamura, T., Yamazaki, K., Iwamoto, K., Honda, M., Miyoshi, Y., Ogawa, Y., Tomikawa, Y., and Ukita, J.: The stratospheric pathway for Arctic impacts on midlatitude climate, *Geophysical Research Letters*, 43, 3494–3501, <https://doi.org/10.1002/2016GL068330>, 2016.

Nghiem, S. V., Hall, D. K., Mote, T. L., Tedesco, M., Albert, M. R., Keegan, K., Shuman, C. A., DiGirolamo, N. E., and Neumann, G.: The extreme melt across the Greenland ice sheet in 2012, *Geophys. Res. Lett.*, 39, 2012GL053611, <https://doi.org/10.1029/2012GL053611>, 2012.

Nowack, P., Runge, J., Eyring, V., and Haigh, J. D.: Causal networks for climate model evaluation and constrained projections, *Nat Commun*, 11, 1415, <https://doi.org/10.1038/s41467-020-15195-y>, 2020.

O’Gorman, P. A.: Contrasting responses of mean and extreme snowfall to climate change, *Nature*, 512, 416–418, <https://doi.org/10.1038/nature13625>, 2014.

Overland, J. E. and Wang, M.: Impact of the winter polar vortex on greater North America, *Intl Journal of Climatology*, 39, 5815–5821, <https://doi.org/10.1002/joc.6174>, 2019.

Pfleiderer, P., Schleussner, C.-F., Geiger, T., and Kretschmer, M.: Robust predictors for seasonal Atlantic hurricane activity identified with causal effect networks, *Weather Clim. Dynam.*, 1, 313–324, <https://doi.org/10.5194/wcd-1-313-2020>, 2020.

Preece, J. R., Mote, T. L., Cohen, J., Wachowicz, L. J., Knox, J. A., Tedesco, M., and Kooperman, G. J.: Summer atmospheric circulation over Greenland in response to Arctic amplification and diminished spring snow cover, *Nat Commun*, 14, 3759, <https://doi.org/10.1038/s41467-023-39466-6>, 2023.

Previdi, M., Smith, K. L., and Polvani, L. M.: Arctic amplification of climate change: a review of underlying mechanisms, *Environ. Res. Lett.*, 16, 093003, <https://doi.org/10.1088/1748-9326/ac1c29>, 2021.

Quante, L., Willner, S. N., Middelani, R., and Levermann, A.: Regions of intensification of extreme snowfall under future warming, *Sci Rep*, 11, 16621, <https://doi.org/10.1038/s41598-021-95979-4>, 2021.

Runge, J.: Causal network reconstruction from time series: From theoretical assumptions to practical estimation, *Chaos*, 28, 075310, <https://doi.org/10.1063/1.5025050>, 2018.

Runge, J., Nowack, P., Kretschmer, M., Flaxman, S., and Sejdinovic, D.: Detecting and quantifying causal associations in large nonlinear time series datasets, *Sci. Adv.*, 5, eaau4996, <https://doi.org/10.1126/sciadv.aau4996>, 2019a.

Deleted: 32

Formatted: Font colour: Black

Formatted: Normal, Border: Top: (No border), Bottom: (No border), Left: (No border), Right: (No border), Between : (No border), Tab stops: 7.96 cm, Centred + 15.92 cm, Right

1404 Runge, J., Bathiany, S., Bollt, E., Camps-Valls, G., Coumou, D., Deyle, E., Glymour, C., Kretschmer, M., Mahecha, M. D.,
1405 Muñoz-Mari, J., van Nes, E. H., Peters, J., Quax, R., Reichstein, M., Scheffer, M., Schölkopf, B., Spirtes, P., Sugihara, G.,
1406 Sun, J., Zhang, K., and Zscheischler, J.: Inferring causation from time series in Earth system sciences, *Nat Commun*, 10, 2553,
1407 <https://doi.org/10.1038/s41467-019-10105-3>, 2019b.

1408 Sasgen, I., Wouters, B., Gardner, A. S., King, M. D., Tedesco, M., Landerer, F. W., Dahle, C., Save, H., and Fettweis, X.:
1409 Return to rapid ice loss in Greenland and record loss in 2019 detected by the GRACE-FO satellites, *Commun Earth Environ*,
1410 1, 8, <https://doi.org/10.1038/s43247-020-0010-1>, 2020.

1411 Scaife, A.A., Smith, D. A signal-to-noise paradox in climate science. *npj Clim Atmos Sci* 1, 28 (2018).
1412 <https://doi.org/10.1038/s41612-018-0038-4>

1413 Scherrer, S. C., Croci-Maspoli, M., Schwierz, C., and Appenzeller, C.: Two-dimensional indices of atmospheric blocking and
1414 their statistical relationship with winter climate patterns in the Euro-Atlantic region, *Int. J. Climatol.*, 26, 233–249,
1415 <https://doi.org/10.1002/joc.1250>, 2006.

1416 Screen, J. A., Deser, C., Smith, D. M., Zhang, X., Blackport, R., Kushner, P. J., Oudar, T., McCusker, K. E., and Sun, L.:
1417 Consistency and discrepancy in the atmospheric response to Arctic sea-ice loss across climate models, *Nature Geosci*, 11, 155–
1418 163, <https://doi.org/10.1038/s41561-018-0059-y>, 2018.

1419 Serreze, M. C., Barrett, A. P., Stroeve, J. C., Kindig, D. N., and Holland, M. M.: The emergence of surface-based Arctic
1420 amplification, *The Cryosphere*, 2009.

1421 Shang, Y., Liu, P., and Wu, S.: Responses of the Pacific and Atlantic decadal variabilities under global warming by using
1422 CMIP6 models, *Ocean Dynamics*, 74, 67–75, <https://doi.org/10.1007/s10236-023-01590-8>, 2024.

1423 Shepherd, Andrew, Ivins, Erik, Rignot, Eric, Smith, Ben, van den Broeke, Michiel, Velicogna, Isabella, Whitehouse, Pippa,
1424 Briggs, Kate, Joughin, Ian, Krinner, Gerhard, Nowicki, Sophie, Payne, Antony, Scambos, Ted, Schlegel, Nicole, A. Geruo,
1425 Agosta, Cécile, Ahlstrom, Andreas, Babonis, Greg, Barletta, Valentina, Bjørk, Anders, Blazquez, Alejandro, Bonin, Jennifer,
1426 Colgan, William, Csatho, Beata, Cullather, Richard, Engdahl, Marcus, Felikson, Denis, Fettweis, Xavier, Forsberg, René,
1427 Galée, Hubert, Gardner, Alex, Gilbert, Lin, Gourmelen, Noel, Groh, Andreas, Gunter, Brian, Hanna, Edward, Harig,
1428 Christopher, Helm, Veit, Hogg, Anna, Horvath, Alexander, Horwath, Martin, Khan, Shfaqat, Kjeldsen, Kristian, Konrad,
1429 Hannes, Langen, Peter, Lecavalier, Benoit, Loomis, Bryant, Luthcke, Scott, McMillan, Malcolm, Melini, Daniele, Mernild,
1430 Sebastian, Mohajerani, Yara, Moore, Philip, Mottram, Ruth, Mouginot, Jeremie, Moyano, Gorka, Muir, Alan, Nagler, Thomas,
1431 Nield, Grace, Nilsson, Johan, Noël, Brice, Otosaka, Inès, Pattle, Mark, Peltier, W. Pie, Nadège, Rietbroek, Roelof, Rott,
1432 Helmut, Sørensen, Louise Sandberg, Sasgen, Ingo, Save, Himanshu, Scheuchl, Bernd, Schrama, Ernst, Schröder, Ludwig, Seo,
1433 Ki-Weon, Simonsen, Sebastian, Slater, Thomas, Spada, Giorgio, Sutterley, Tyler, Talpe, Matthieu, Tarasov, Lev, van de Berg,
1434 Willem Jan, van der Wal, Wouter, van Wessem, Melchior, Vishwakarma, Bramha Dutt, Wagner, Thomas, Wiese, David,
1435 Wilton, David, Wouters, Bert, and Wuite, Jan: Antarctic and Greenland Ice Sheet mass balance 1992-2020 for IPCC AR6
1436 (1.0), <https://doi.org/10.5285/77B64C55-7166-4A06-9DEF-2E400398E452>, 2021.

1437 Shu, Q., Wang, Q., Årthun, M., Wang, S., Song, Z., Zhang, M., and Qiao, F.: Arctic Ocean Amplification in a warming climate
1438 in CMIP6 models, *Sci. Adv.*, 8, eabn9755, <https://doi.org/10.1126/sciadv.abn9755>, 2022.

1439 Tedesco, M. and Fettweis, X.: Unprecedented atmospheric conditions (1948–2019) drive the 2019 exceptional melting season
1440 over the Greenland ice sheet, *The Cryosphere*, 14, 1209–1223, <https://doi.org/10.5194/tc-14-1209-2020>, 2020.

1441 Tedesco, M., Fettweis, X., van den Broeke, M. R., van de Wal, R. S. W., Smeets, C. J. P. P., van de Berg, W. J., Serreze, M.
1442 C., and Box, J. E.: The role of albedo and accumulation in the 2010 melting record in Greenland, *Environ. Res. Lett.*, 6, 014005,
1443 <https://doi.org/10.1088/1748-9326/6/1/014005>, 2011.

Deleted: 33

Formatted: Font colour: Black

Formatted: Normal, Border: Top: (No border), Bottom: (No border), Left: (No border), Right: (No border), Between : (No border), Tab stops: 7.96 cm, Centred + 15.92 cm, Right

1444 Tian, Y., Giaquinto, D., Di Capua, G. et al.: Historical changes in the Causal Effect Networks of compound hot and dry
1445 extremes in central Europe. *Commun Earth Environ* 5, 764 (2024). <https://doi.org/10.1038/s43247-024-01934-2>

1446 Tibaldi, S. and Molteni, F.: On the operational predictability of blocking. *Tellus A*, 42, 343–365,
1447 <https://doi.org/10.1034/j.1600-0870.1990.t01-2-00003.x>, 1990.

1448 Tyrllis E, Bader J, Manzini E, Matei D. Reconciling different methods of high-latitude blocking detection. *Q J R Meteorol Soc.*
1449 2021; 147: 1070–1096. <https://doi.org/10.1002/qj.39>

1450 Topál, D., Ding, Q., Ballinger, T. J., Hanna, E., Fettweis, X., Li, Z., and Pieczka, I.: Discrepancies between observations and
1451 climate models of large-scale wind-driven Greenland melt influence sea-level rise projections, *Nat Commun*, 13, 6833,
1452 <https://doi.org/10.1038/s41467-022-34414-2>, 2022.

1453 Wachowicz, L. J., Preece, J. R., Mote, T. L., Barrett, B. S., and Henderson, G. R.: Historical trends of seasonal Greenland
1454 blocking under different blocking metrics, *Intl Journal of Climatology*, 41, <https://doi.org/10.1002/joc.6923>, 2020.

1455 Wang, H. and Luo, D.: North Atlantic Footprint of Summer Greenland Ice Sheet Melting on Interannual to Interdecadal Time
1456 Scales: A Greenland Blocking Perspective, *Journal of Climate*, 35, 1939–1961, <https://doi.org/10.1175/JCLI-D-21-0382.1>,
1457 2022.

1458 Wang, S. S., Huang, W., and Yoon, J.: The North American winter ‘dipole’ and extremes activity: a CMIP5 assessment,
1459 *Atmospheric Science Letters*, 16, 338–345, <https://doi.org/10.1002/asl2.565>, 2015.

1460 Woollings, T. and Hoskins, B.: Simultaneous Atlantic–Pacific blocking and the Northern Annular Mode, *Quart J Royal*
1461 *Meteoro Soc*, 134, 1635–1646, <https://doi.org/10.1002/qj.310>, 2008.

1462 Woollings, T., Barriopedro, D., Methven, J., Son, S.-W., Martius, O., Harvey, B., Sillmann, J., Lupo, A. R., and Seneviratne,
1463 S.: Blocking and its Response to Climate Change, *Curr Clim Change Rep*, 4, 287–300, [https://doi.org/10.1007/s40641-018-](https://doi.org/10.1007/s40641-018-0108-z)
1464 [0108-z](https://doi.org/10.1007/s40641-018-0108-z), 2018.

1465 Ye, K. and Jung, T.: How Strong Is Influence of the Tropics and Midlatitudes on the Arctic Atmospheric Circulation and
1466 Climate Change?, *Geophysical Research Letters*, 46, 4942–4952, <https://doi.org/10.1029/2019GL082391>, 2019.

1467 Zhang, B., Liu, L., Khan, S. A., van Dam, T., Bjørk, A. A., Peings, Y., Zhang, E., Bevis, M., Yao, Y., and Noël, B.: Geodetic
1468 and model data reveal different spatio-temporal patterns of transient mass changes over Greenland from 2007 to 2017, *Earth*
1469 *and Planetary Science Letters*, 515, 154–163, <https://doi.org/10.1016/j.epsl.2019.03.028>, 2019.

1470 Zhu, Z., Lu, R., Yu, B., Li, T., and Yeh, S.-W.: A moderator of tropical impacts on climate in Canadian Arctic Archipelago
1471 during boreal summer, *Nat Commun*, 15, 8644, <https://doi.org/10.1038/s41467-024-53056-0>, 2024

Formatted: Space After: 12 pt, Border: Top: (No border), Bottom: (No border), Left: (No border), Right: (No border), Between : (No border)

Deleted: 34

Formatted: Font colour: Black

Formatted: Normal, Border: Top: (No border), Bottom: (No border), Left: (No border), Right: (No border), Between : (No border), Tab stops: 7.96 cm, Centred + 15.92 cm, Right

Page 1: [1] Formatted	Author	28/07/2025 12:25:00
------------------------------	---------------	----------------------------

Normal, Border: Top: (No border), Bottom: (No border), Left: (No border), Right: (No border), Between : (No border), Tab stops: 7.96 cm, Centred + 15.92 cm, Right

Page 2: [2] Deleted	Author	28/07/2025 12:25:00
----------------------------	---------------	----------------------------

▼

Page 2: [3] Deleted	Author	28/07/2025 12:25:00
----------------------------	---------------	----------------------------

▼

Page 2: [4] Deleted	Author	28/07/2025 12:25:00
----------------------------	---------------	----------------------------

▼

Page 2: [5] Deleted	Author	28/07/2025 12:25:00
----------------------------	---------------	----------------------------

▼

Page 15: [6] Deleted	Author	28/07/2025 12:25:00
-----------------------------	---------------	----------------------------

▼

Page 15: [6] Deleted	Author	28/07/2025 12:25:00
-----------------------------	---------------	----------------------------

▼

Page 15: [6] Deleted	Author	28/07/2025 12:25:00
-----------------------------	---------------	----------------------------

▼

Page 15: [6] Deleted	Author	28/07/2025 12:25:00
-----------------------------	---------------	----------------------------

▼

Page 15: [7] Deleted	Author	28/07/2025 12:25:00
-----------------------------	---------------	----------------------------

▼

Page 15: [7] Deleted	Author	28/07/2025 12:25:00
-----------------------------	---------------	----------------------------

▼

Page 15: [7] Deleted	Author	28/07/2025 12:25:00
-----------------------------	---------------	----------------------------

▼

Page 15: [8] Deleted	Author	28/07/2025 12:25:00
-----------------------------	---------------	----------------------------

▼

Page 15: [8] Deleted	Author	28/07/2025 12:25:00
-----------------------------	---------------	----------------------------

▼

Page 27: [9] Deleted	Author	28/07/2025 12:25:00
-----------------------------	---------------	----------------------------

▼

